AD-A085 715 KAMAN AVIDYNE BURLINGTON MA F/G 18/3
PIVUL - A COMPUTER CODE FOR RAPID ASSESSMENT OF THE VULNERABILI--ETC(U)
MAR 80 N P HOBBS, K R WETHORE DAAD05-76-C-0742
UNCLASSIFIED KA-TR-125 ARBRL-CR-00417 NL

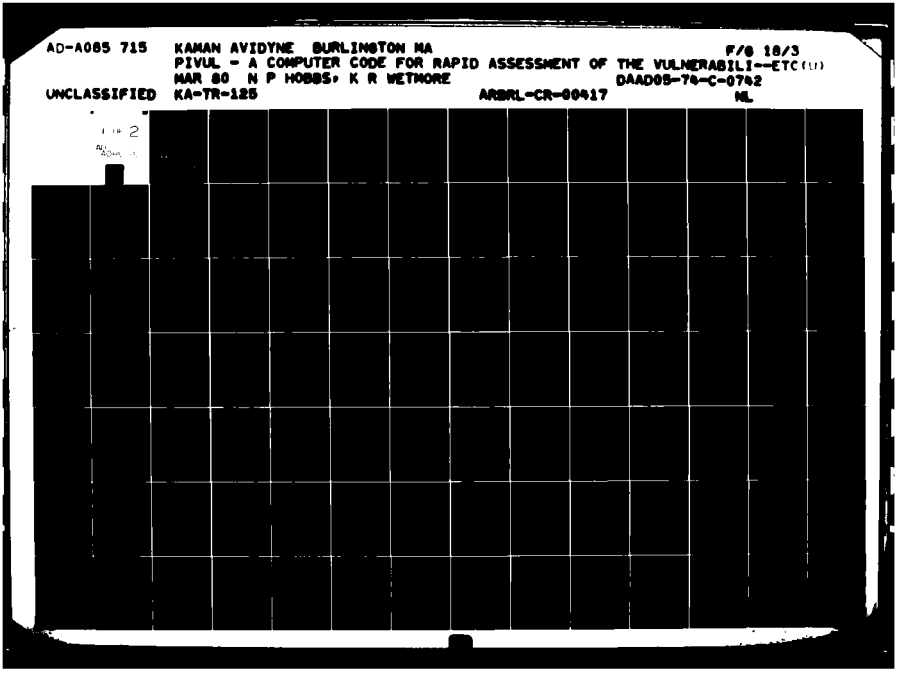

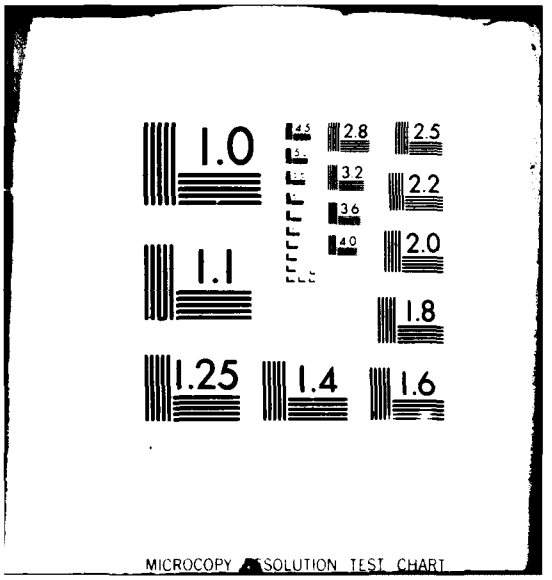
1.0
1.1
1.25
1.4
1.6
1.8
2.0
2.2
2.5
2.8
3.2
3.6
4.0
MICROCOPY RESOLUTION TEST CHART

CONTRACT REPORT ARBRL-CR-00417

PIVUL - A COMPUTER CODE FOR RAPID ASSESSMENT OF THE VULNERABILITY OF SIMPLE STRUCTURES TO BLAST

Prepared by

Kaman AviDyne
A Division of
Kaman Sciences Corporation
Burlington, MA 01803

March 1980

US ARMY ARMAMENT RESEARCH AND DEVELOPMENT COMMAND
BALLISTIC RESEARCH LABORATORY
ABERDEEN PROVING GROUND, MARYLAND

Destroy this report when it is no longer needed.
Do not return it to the originator.

Secondary distribution of this report by originating or sponsoring activity is prohibited.

Additional copies of this report may be obtained from the National Technical Information Service, U.S. Department of Commerce, Springfield, Virginia 22151.

The findings in this report are not to be construed as an official Department of the Army position, unless so designated by other authorized documents.

The use of trade names or manufacturers' names in this report does not constitute indorsement of any commercial product.

UNCLASSIFIED

SECURITY CLASSIFICATION OF THIS PAGE (When Data Entered)

REPORT DOCUMENTATION PAGE	READ INSTRUCTIONS BEFORE COMPLETING FORM
1. REPORT NUMBER CONTRACT REPORT ARBRL-CR-00417 ✓	2. GOVT ACCESSION NO. AD-A085 715
3. RECIPIENT'S CATALOG NUMBER	
4. TITLE (and Subtitle) PIVUL - A COMPUTER CODE FOR RAPID ASSESSMENT OF THE VULNERABILITY OF SIMPLE STRUCTURES TO BLAST	5. TYPE OF REPORT & PERIOD COVERED Final Report - Jan. 14, 1974 through August 31, 1975
	6. PERFORMING ORG. REPORT NUMBER KA TR-125 ✓
7. AUTHOR(s) Norman P. Hobbs Kenneth R. Wetmore	8. CONTRACT OR GRANT NUMBER(s) DAAD05-74-C-0742
9. PERFORMING ORGANIZATION NAME AND ADDRESS Kaman AviDyne ✓ A Division of Kaman Sciences Corporation Burlington, MA 01803	10. PROGRAM ELEMENT, PROJECT, TASK AREA & WORK UNIT NUMBERS
11. CONTROLLING OFFICE NAME AND ADDRESS U.S. Army Armament Research & Development Command U.S. Army Ballistic Research Laboratory ATTN: DRDAR-BL Aberdeen Proving Ground, MD 21005	12. REPORT DATE MARCH 1980 13. NUMBER OF PAGES 109
14. MONITORING AGENCY NAME & ADDRESS (if different from Controlling Office) U.S. Army Materiel Development & Readiness Command 5001 Eisenhower Avenue Alexandria, VA 22333	15. SECURITY CLASS. (of this report) UNCLASSIFIED 15a. DECLASSIFICATION DOWNGRADING SCHEDULE

16. DISTRIBUTION STATEMENT (of this Report)

Approved for public release; distribution unlimited.

17. DISTRIBUTION STATEMENT (of the abstract entered in Block 20, if different from Report)

G 27044

18. SUPPLEMENTARY NOTES

This research was sponsored by the Defense Nuclear Agency under Subtask V99QAXNB005, Work Unit Code 05, Military Equipment Vulnerability.

19. KEY WORDS (Continue on reverse side if necessary and identify by block number)

Pressure-impulse
Blast damage of simple structures
Vulnerability code

20. ABSTRACT (Continue on reverse side if necessary and identify by block number)

This report presents the methodology which led to the development of a vulnerability code, PIVUL, for utilization in rapid damage assessment of simple structural elements subjected to a nuclear blast environment. The basic concept of blast damage assessment employed in the report is the pressure-impulse approach. Light, moderate, and heavy damage are considered.

DD FORM 1 JAN 73 1473 EDITION OF 1 NOV 65 IS OBSOLETE

UNCLASSIFIED

SECURITY CLASSIFICATION OF THIS PAGE (When Data Entered)

FOREWORD

This is the final report on the project entitled "Pressure-Impulse Blast Program" performed at Kaman AviDyne, Burlington, Mass., for the Ballistic Research Laboratories under Contract No. DAAD05-74-C-0742. Drs. Benjamin Cummings and William Schuman, Jr. were the technical monitors for BRL.

The study was performed in the Structural Mechanics Group of Kaman AviDyne headed by Mr. E.S. Criscione and the authors wish to thank Mr. Criscione for his technical assistance. The authors also wish to thank Mr. Michael Tomayko of the Kaman AviDyne Computing Staff for his extensive efforts in conducting the required computer case studies.

TABLE OF CONTENTS

TABLE OF CONTENTS (Concluded)

LIST OF ILLUSTRATIONS

LIST OF TABLES

SECTION 1
INTRODUCTION

Many different military targets must be analyzed with regard to their vulnerability to the blast effects from a nuclear weapon. Often these targets are comprised of structural elements such as plates, beams, and cylindrical bodies. A convenient, simple, and approximate means of defining the vulnerability of a structural element is by Pressure (P) - Impulse (I) curves for different levels of damage. In the past these P-I curves have been generated experimentally at considerable cost. The same sort of thing can be accomplished by using complex computer codes. Consequently, the basic objectives of the current study are the following: 1) to develop P-I curves from complex computer codes for different structural shapes such as beams, plates, and cylinders for three levels of damage - light, moderate, and severe, and 2) to include these P-I curves in a computer code which the analyst can use to rapidly approximate the vulnerability of a specific target to blast.

The response of structural systems to nuclear blast effects has been of interest to the military community for many years and past efforts aimed at assessing structural blast damage have involved both experimental and analytical approaches. Since full-scale structural blast damage response cannot be measured until the structural system has been built and experiments performed, experimental studies tend to be expensive, particularly if tests of a variety of structural configurations and damage levels are required. On the other hand, analytical assessment of structural blast damage can be accomplished either after the actual structure has been built or before production, while the structure is still in the design stage. Thus, it is evident that the availability of analytical data for different damage levels of structural blast response on a variety of structural configurations would certainly be of interest to both weapon systems designers and analysts, particularly for quick-look vulnerability assessment. Consequently, the U.S. Army Ballistic Research Laboratories sponsored the present analytical blast study program whose ultimate objective was to make such data readily available.

The basic analytical technique which was selected to provide the required blast damage assessment data was the pressure-impulse approach which had proven quite successful in previous structural blast damage assessment. Section 2 of this report provides a background discussion of the pressure-impulse approach and its application to the proposed program objective. As specified in the contract statement of work, the first detailed requirement of the program was to review selected military structural configurations and to select typical simple structural shapes which could be interpreted as representative component shapes

for those systems. Once the representative component shapes were chosen, the next step specified was to determine what response/damage levels, materials, boundary conditions, and loading functions would be of interest in evaluating blast effects on those representative components and to utilize appropriate computer codes in conjunction with the pressure-impulse approach to calculate the required response data. In Section 3 of the report, descriptions are given of the type, scope and limitations of the pressure-impulse analyses which were undertaken. These descriptions include, among other things, the types of and constraints on the structural component models considered, the applicability of the assumed loading functions, the computer codes employed in the structural response investigations, and the implementation of the basic pressure-impulse approach.

Section 4 presents an explanation of the manner in which analytical fitting functions were used to process the derived pressure-impulse data into a form suitable for incorporation into the vulnerability computer code which was formulated as the specified end requirement of the contract. A description of the code together with an explanation of its usage for rapid assessment of blast structural vulnerability is presented in Section 5. Finally, Section 6 presents the conclusions and recommendations.

SECTION 2
PRESSURE-IMPULSE APPROACH TO STRUCTURAL BLAST DAMAGE DEFINITION

The response of military structures to nuclear weapon effects has been of interest ever since the first atomic weapon was introduced into the offensive weapon arsenal. In particular, military strategists have been faced with the problem of assessing the size of nuclear weapons needed to destroy the enemy's offensive and defensive capabilities and, conversely, how to assess the hardness of one's own military structures to nuclear weapons effects.

The work reported herein describes one study effort performed to improve the capability for rapid prediction of damage to military equipment caused by the blast effects resulting from nuclear weapons detonations. More specifically, the intent of the study is to provide nuclear blast effects methodology which can be utilized in either preliminary design of structural systems for blast effects or in making a rapid assessment of nuclear blast damage to existing structural systems.

The basic concept of blast effects damage assessment employed in the present report is the pressure-impulse approach for relating dynamic structural response/damage to structural blast loadings created by nuclear weapons detonations. As will be subsequently discussed, the pressure-impulse approach, hereafter referred to as the P-I approach, is not a new concept in structural damage assessment but has been used for many years by structural analysts interested in structural blast damage assessment.

In structural analysis, the response of a particular structural item is functionally dependent on many parameters, including the geometry of the structural item, the material used, the structural support fixity, and the nature of the loading. If the load imposed on the structure does not vary with time, the structure may be analyzed as a static structure and handbook formulas are often available for determining the structural deformation as a function of the magnitude and spatial distribution of the applied load. On the other hand, if the load imposed on the structure is time-varying then dynamic structural analysis is required since the response is functionally dependent on the temporal variation of the loading as well as the dynamic characteristics of the structure. It is the latter case which is of interest in the present report since the blast-type loadings which are of interest in this program are dynamic loadings rather than static loadings.

The detonation of an explosive charge creates a shock front or blast wave which propogates radially outward from the center of the detonation. It is not the intent of this report to present a detailed explanation of shock-wave propagation and it suffices to say that at the advancing shock front there is an almost instantaneous increase in air pressure above the ambient air pressure, called the overpressure.

As the distance from the detonation center increases, the peak overpressure decreases. At a given distance, the magnitude of the overpressure behind the shock front decreases with increasing time after detonation, so that the time-history of the pressure experienced at a point might appear as depicted in Figure 2.1, where the overpressure is plotted versus the time after detonation. The time t_1 represents the time required for the shock front to travel from the detonation center to the point in question, the time t_2 represents the positive phase of the pressure pulse (i.e., the time duration for which the pressure is greater than ambient pressure), and time t_3 represents the negative phase of the pressure pulse during which time the pressure is less than ambient pressure. In this report, only the positive phase of the overpressure-time history is of significance and, hence, only blast loadings corresponding to the time period t_2 in Figure 2.1 are considered. The blast loadings of interest, then, are seen to be pressure loadings which change over a finite time period and are dynamic rather than static in character.

If the typical positive phase pressure loading depicted in Figure 2.1 is applied to a particular structural item, such as a fixed-end beam for instance, the deformation pattern of the beam will vary with time since, as previously indicated, the dynamic response is a function of both the dynamic characteristics of the structure and the time-history of the loading function. Within some finite period of the structural response, however, maximum values of deflections, strains and stresses will be reached and the maximum amount of damage which is incurred on the structure can be related to one of the maximum response quantities. If the same structure is subjected to another pressure pulse of the form depicted in Figure 2.1 but with a di .erent magnitude of either peak overpressure or positive duration, the maximum value of the same response parameter will differ from the peak value experienced during the original loading. There are, however, other combinations of peak overpressure and positive duration that will result in the same peak response or peak damage level as that obtained from the original loading.

Referring back to the loading depicted in Figure 2.1, to be more consistent with the literature, Δp_{max} will henceforth be referred to as Δp_s, the value of overpressure at the shock front, and t_2 will be referred to as t_o, the positive phase duration. Since, as shown in Figure 2.1, the overpressure at a point removed from the detonation center decays in an exponential manner with time, an expression for the overpressure as a function of time may be written as

$$\Delta p(t) = \Delta p_s \left(1 - \frac{t}{t_o}\right) e^{-t/t_o} \qquad (2.1)$$

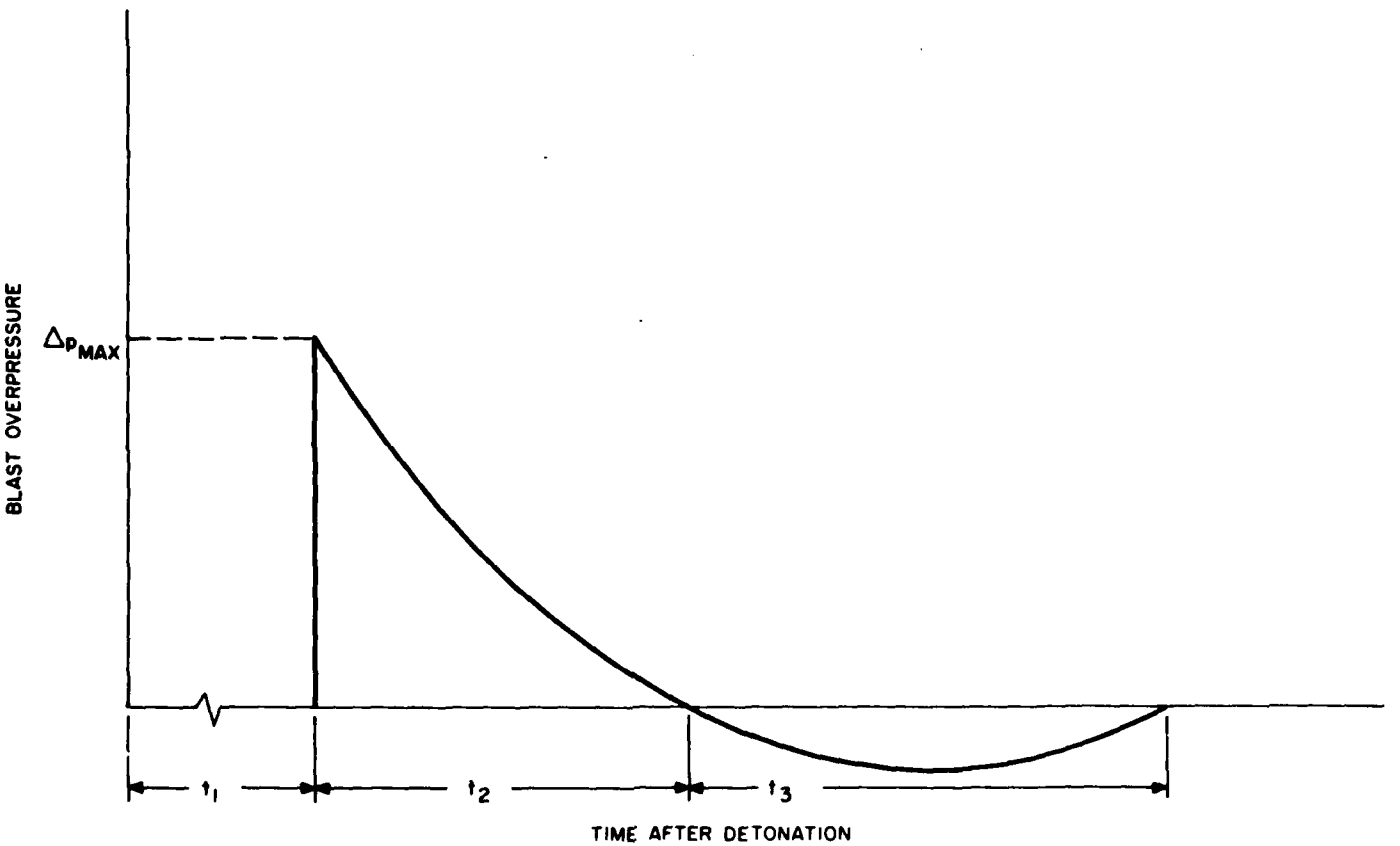

FIGURE 2.1 BLAST OVERPRESSURE-TIME PLOT AT A FIXED POINT IN SPACE

where t=0 corresponds to the shock front arrival at the point. It can be seen then that the entire loading time-history curve can be defined by only two parameters, Δp_s and t_o. It would be entirely possible then to load the identical structure with the same forcing function of Eq. (2.1), but with varying combinations of Δp_s and t_o, and determine the combinations of the two parameters which would result in the same response level. The plot of these various Δp_s and t_o pairs would then define a curve of equivalent level of response or damage, commonly referred to as an iso-damage curve.

For forcing functions of a more general shape than that expressed by Eq. (2.1), a greater number of parameters are required to define the loading time-history. Noting that the response will depend upon any parameter which affects the loading time-history (up to the time of maximum response), it becomes apparent that the response will then depend upon more than two parameters for an arbitrary loading time-history. The construction of iso-damage curves depending upon more than two parameters becomes cumbersome, however. Efforts in the P-I area have been directed toward selecting the two most dominant loading parameters in the hope that the influence of the unused parameters will be small.

The most fundamental approach originated in the work of Sperrazza (Ref. 1) in 1951. Sperrazza based his iso-damage curves on the two key parameters of peak pressure of the forcing function and the total impulse associated with the forcing function time history, hence the resulting name pressure-impulse (P-I) approach. In a later study reported in Ref. 2, Youngdahl noted that the structural response was strongly dependent on the shape of the forcing function even for pulses which have the same total impulse and peak pressure, which is implied by the foregoing comments. In his paper, Youngdahl suggested the use of an "effective pressure" and an "effective impulse", showing that, in some sense, these two parameters represented a better choice than peak pressure and fatal impulse. Certain procedural difficulties occur in employing Youngdahl's definitions of effective pressure and effective impulse. Hence, in a later study, Ref. 3, Cummings and Schumacher suggest a simplified version of Youngdahl's approach, in which the "effective pressure" and "effective impulse" are redefined by changing the integration limits involved. This approach, along with the fundamental P-I approach employing peak pressure and total impulse, is used in the present study.

Ref. 1. Sperrazza, J., Dependence of External Blast Damage to the A-25 Aircraft on Peak Pressure and Impulse, Memorandum Report 575, USA Ballistic Research Laboratories, APG, Maryland, September 1951. (AD#378275)

Ref. 2. Youngdahl, C.K., "Correlation Parameters for Eliminating the Effect of Pulse Shape on Dynamic Plastic Deformation", Journal of Applied Mechanics, Transactions of the ASME, pp. 744-752, September 1970.

Ref. 3. Schumacher, R., and Cummings, B., A Modified Pressure-Impulse Blast Damage Model, BRL MR 2724, AD No. A036196, USA Ballistic Research Laboratory, APG, Maryland, January 1977.

It is important to recognize that any response which is found as a function of only two parameters of an arbitrary loading can be only an approximation to the true response. If iso-damage curves calculated based upon the loading time-history of Eq. (2.1) are applied for loading time-histories with similar characteristics, the approximation will be good. If they were applied, for example, to a half sine-wave forcing function, the approximation would be expected to be poor. The data generated are based upon the loading time-history of Eq. (2.1), and must therefore be applied only to similar loadings. Since blast loadings, even including reflection-diffraction effects, are basically similar to that given by Eq. (2.1), the approximation involved in the present context in ignoring the complete details of the loading time-history should be acceptable. Appendix A shows the type of variation that may be expected in the P-I curve for different forcing functions within the same class.

SECTION 3
DEVELOPMENT OF P-I CURVES

3.1 Introduction

As indicated in Section 1, the primary objectives of the technical effort reported herein were to develop P-I curves for simple structural elements subjected to nuclear blast overpressure loadings and to include these P-I curves in a vulnerability assessment code. A description of the structural elements selected for analysis, the modeling of the elements including the boundary conditions and materials assumed, the assumed aerodynamic loading functions, the selection of the response damage criteria, and the methods of response analysis are discussed in the first portion of this section. The remainder of the section is primarily devoted to the formulation of the P-I curves which were needed for inclusion in the vulnerability code.

3.2 Selection of Typical Structural Models

The process of selecting representative structural items for which P-I curves might be formulated was initiated by reviewing several different Army weapon system configurations. Drawings of the UH-1B helicopter, the S-280 electronic equipment shelter, and the M-113 personnel carrier were studied to determine what simple structural elements comprising these systems or other systems might be considered as representative or typical items for analysis. During the reviewing period, particular attention was given to the geometry of both primary and secondary structure, such as exterior skin panels which would be exposed to blast effects and interior back-up structure.

Typical panel sizes, expressed as length-to-width ratios, range from 2-4 for the M-113 personnel carrier, from 2.5-5 for the UH-1B helicopter, and as much as 2-8 for the S-280 electronic equipment shelter. Typical panel thicknesses show a wide variance among the three weapon systems reviewed. The M-113 typical panels may be characterized as single-layered thick flat plates of homogeneous material, ranging in thickness from 31.8 - 44.5 mm. The UH-1B helicopter panels, on the other hand, are single-layered thin curved plates of homogeneous material, varying in thickness from .5 - 1.3 mm. For the S-280 shelter, typical skin panels are of heterogeneous sandwich construction with a typical thickness on the order of 52 mm.

The primary panel support or back-up structure for the S-280 shelter is a brace in the form of a hat-section extrusion. Typical of aircraft semi-monocoque construction, the UH-1B back-up structure, consisting of frames, longerons, and stringers, is comprised of a variety of extrusions of varying length and cross-sectional geometry. Due to the thick plate, welded construction employed in the M-113 personnel carrier, secondary or back-up structure is virtually non-existent.

The choice of the range of geometrical parameters for the various types of structural models to be analyzed was relatively uncomplicated except for the beam structural models. For the cylinder, the response is a function of two geometrical ratios, the length to radius ratio and the radius to thickness ratio. For flat plates, the response is a function of the length-to-width and width-to-thickness ratios of the plate. For straight beams, however, the response depends upon the length and the cross-sectional configuration.

As previously mentioned, the backup structures for the Army weapon systems reviewed consisted of a variety of structural elements such as braces, stringers, longerons, etc., all of which may be generally classified as structural beams. The structural beams which had been looked at in the preliminary review task had cross sections such as depicted in Figure 3.1 and were typical of standard extruded members. Generally speaking, all of these extrusions may be typified as either two- or three-area cross sections, as indicated. Both the two- and three-area cross sections have a top horizontal area A_1 attached to a vertical area A_2, although the bottom horizontal area A_3 may or may not exist depending upon the configuration used. Also, as indicated in Figure 3.1, either area A_2 or area A_3 may be comprised of more than one element. The vertical distribution of the individual areas of a beam cross section and not the horizontal distribution of the areas is the important factor affecting beam vertical bending response.

In order to take advantage of this irrelevancy of the horizontal distribution of individual areas of beam cross sections, it was decided to synthesize one generic beam cross section which could be used to approximate all beam cross sections of interest. The synthesized cross section which was selected for the straight beam model P-I analyses is shown in Figure 3.2. The relative depths chosen for the areas A_1, A_2, and A_3 were based on a review of the pertinent dimensions of typical standard extrusions tabulated in Ref. 4. It was determined from the data given in Ref. 4 that a typical ratio of area A_2 depth to either area A_1 or area A_3 depth was on the order of 18 to 1, and hence this ratio was used in formulating the synthesized cross section. Additionally, it was determined that as long as this ratio is of the order indicated, the beam response will be insensitive to small ratio variations.

The parameters which influence the beam response, exclusive of the parameters defining the material and the time-history of the pressure loading, are the two area ratios A_2/A_1 and A_3/A_1, the length-to-depth ratio L/H, the value of H, the value of area A_1, and the loading width parameter W. Since the values of both A_1 and W in effect simply would alter the magnitude of the beam loading, their values could be selected arbitrarily. The value of H in effect also alters the beam loading and, in addition, affects the time scale. For input simplification purposes, therefore, a value of unity was chosen for W, H, and w_1 and, as can be seen from Figure 3.2, the selection of a value for w_1 immediately fixed the value of A_1. These choices also result in A_1, W, and H (or L) being involved in the scaling parameters used to interpret the response results. In view of the procedures used to process the data in Section 4, this scaling is implicit rather than explicit.

Ref. 4. ALCOA Structural Handbook, Aluminum Company of America, Pittsburgh, Pa., 1958.

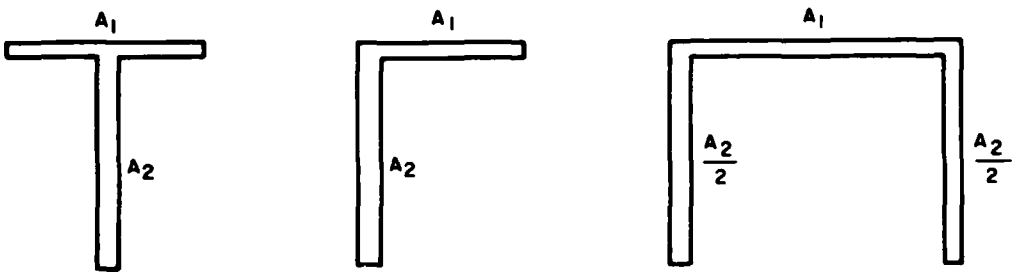

TWO-AREA CROSS SECTIONS

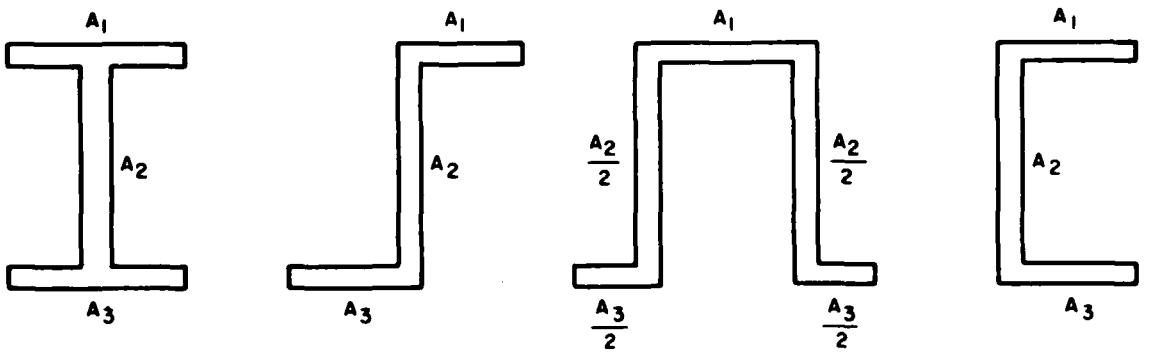

THREE-AREA CROSS SECTIONS

FIGURE 3.1 TYPICAL EXTRUSION CROSS SECTIONS

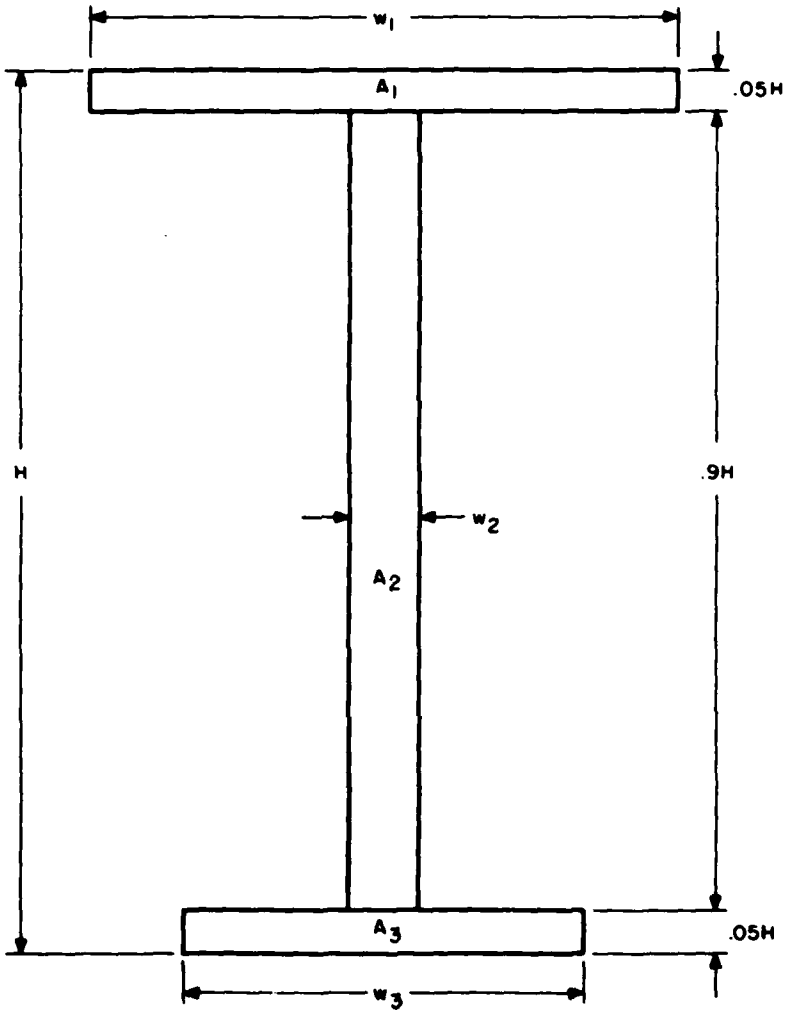

$$\frac{\text{AREA } A_2}{\text{AREA } A_1} = \frac{0.9H\,w_2}{0.05H\,w_1} = 18\frac{w_2}{w_1}$$

$$\frac{\text{AREA } A_3}{\text{AREA } A_1} = \frac{0.05H\,w_3}{0.05H\,w_1} = \frac{w_3}{w_1}$$

FIGURE 3.2 SYNTHESIZED BEAM CROSS SECTION

An examination of the extrusion data in Ref. 4, for both the two-area and three-area cross sections, was then made to determine what ranges of the area ratios indicated on Figure 3.2 should be considered. After having selected specific combinations of area ratios for both two- and three-area beam cross sections, these beam cross-sectional configurations were then combined with selected beam lengths to define the limits of the beam model parameters to be analyzed. In addition, for curved beams various typical radii of curvature were selected as an additional variable parameter.

3.3 Model Boundary Conditions and Materials of Construction

The boundary conditions selected for the structural model response analyses were considered from the standpoint of actual construction techniques, practical simulation by mathematical formulation, and limitations of the existing response codes. Recognizing the fact that the actual support offered to individual beams, panels, and cylinders comprising the types of actual structural systems considered would probably be between the mathematical representations of simple supports and clamped supports, it was adjudged that a clamped support is probably a closer approximation to reality than is a simple support. The decision was made, therefore, to employ a rigidly-fixed support condition for all the types of models to be analyzed.

All of the previously mentioned weapon systems which were reviewed for purposes of selecting typical structural elements for blast response analysis utilize different alloys of aluminum for the primary and secondary structural elements. The M-113 personnel carrier plates are formulated from 5083 aluminum alloy material, the S-280 electronic equipment shelter employs 6061 aluminum alloy both as a part of the outer panel sandwich construction and for the back-up structure extrusions, and the UH-1B helicopter uses 2024 aluminum alloy for the back-up structure and both 2024 aluminum alloy and AZ31B magnesium alloy for the outer skin panels. Another commonly used aluminum alloy for which good stress-strain data are readily available is 7075 aluminum alloy. The decision made jointly by BRL and Kaman AviDyne personnel on the materials to be used in the blast response analyses, therefore, was to consider one 2024 and one 7075 aluminum alloy. Accordingly, 2024-T4 and 7075-T6 were selected as appropriate aluminum alloys for which reasonable amounts of material properties data were readily available.

In both the preliminary response analyses and the final vulnerability code, then, structural elements comprised of either 2024-T4 or 7075-T6 aluminum alloy and rigidly fixed at both ends have been assumed.

3.4 Aerodynamic Loading Functions

3.4.1 Loading on Circular Cylinders

Due to reflection effects which occur when a cylinder is loaded side-on rather than end-on, the side-on orientation is more critical for a given free-field overpressure. Hence, the side-on loading condition will be addressed here.

The side-on loading is characterized by reflection of the shock wave, producing high pressures which are subsequently relieved by diffraction effects. A semi-empirical model for the loading on aircraft fuselages is given in Ref. 5. Loading on a cylinder can easily be derived from this semi-empirical model. It turns out that the time constant of the loading through the reflection and diffraction periods is proportional to the cylinder's radius. The time constant of the structural response of the cylinder is also proportional to the radius. Hence, if response only during the reflection-diffraction period is considered, the physical size of the cylinder makes no difference; only ratios are required.

The semi-empirical method of Ref. 5 remains valid only as long as the blast-wave duration is long in comparison with the reflection-diffraction period. There appears to be no reliable method available for blast-wave durations which are not reasonably long in comparison with the reflection-diffraction period. Furthermore, structural response runs indicate that the peak response of a cylinder occurs during or fairly shortly after the reflection-diffraction period. Hence, with the restriction that the blast-wave duration must be long with respect to the reflection-diffraction period, it makes little difference, as far as the structural response is concerned, how long the blast-wave duration is. With little error, then, the blast wave may be taken as a step function; that is, with infinite positive duration. Thus, the present report will be concerned only with infinite-duration blast waves for cylinders. It must be emphasized that the development and verification of a loading model for short blast-wave durations would require reexamination of the procedure. In the meantime, it can be observed that use of the infinite-duration blast loading will result in overestimating the damage, but probably not by a significant amount for most blast response problems of practical interest.

Earlier, it was indicated that the structural response of a cylinder (in terms of dimensionless quantities, such as strain) is independent of the size of the cylinder during the reflection-diffraction period. The restriction to infinite duration blast waves extends this conclusion to the entire loading period. Hence, the computer runs can be made for the actual cylinder loading, rather than for an arbitrary load-time history which would require interpretation through pressure-impulse considerations for the actual loading. Stated differently, the present study of cylinders is restricted to a single loading time history; hence, no requirement exists for estimating the response to one loading time history from calculated response to a different time history - the actual time history can be used to calculate the response in the first place.

Ref. 5. NOVA - A Digital Computer Program for Calculating the Response of Aircraft to the Overpressure from a Nuclear Weapon, Vol. I - Theory and Program Description, Prepared by Kaman AviDyne for th AFWL, AFWL-TR-72-115, Vol. I, July 1973.

Attention is accordingly directed toward defining the loading time history for a blast wave of infinite duration based on the semi-empirical method for fuselage loadings in Ref. 5. The method of Ref. 5 is more comprehensive than required here, since it treats arbitrary blast-structure orientations rather than just side-on and because it deals with non-cylindrical shapes which may have a forward velocity. The forward velocity makes no difference for a right circular cylinder.

The typical time history of the pressure on the cylinder is shown in Figure 3.3. The shock front arrives at time t_a, which is a function of the angle θ, defined in the insert in Figure 3.3. With zero time defined as the time at which the shock front first reaches any point on the cylinder,

$$t_a = \frac{R(1-\cos\theta)}{V_s} \tag{3.1}$$

where

R is the cylinder radius

V_s is the shock front velocity

The blast wave may be characterized by the overpressure associated with it, Δp_s. The shock strength is defined as

$$\xi \equiv \frac{\Delta p_s}{p_o} \tag{3.2}$$

where

p_o is the ambient pressure

The shock velocity may be found from the shock strength using the Rankine-Hugoniot relation

$$\frac{V_s}{c_o} = \sqrt{\frac{7+6\xi}{7}} \tag{3.3}$$

where c_o is the ambient speed of sound.

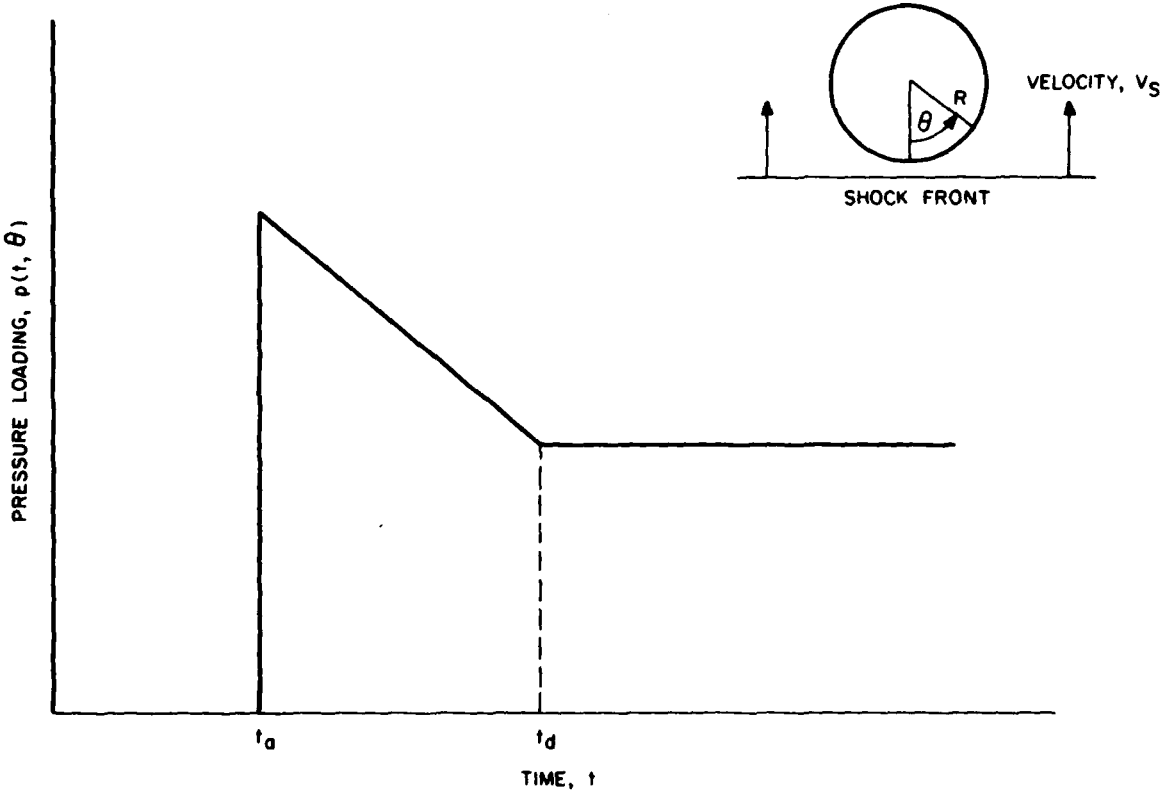

FIGURE 3.3 CYLINDER LOADING TIME HISTORY

The time t_d in Figure 3.3 is the time at which the reflection-diffraction effects end. The loading is taken as linear from t_a to t_d. From Ref. 5

$$t_d = \frac{R(1-\cos\theta)}{V_s - a_{bs}} \tag{3.4}$$

where a_{bs} is the speed of sound behind the shock front, and is given by

$$\frac{a_{bs}}{c_o} = \sqrt{\frac{(1+\xi)(7+\xi)}{7+6\xi}} \tag{3.5}$$

Equation (3.4) results in $t_d = 0$ for $\theta = 0$. This is not correct, and to avoid this situation, Ref. 5 introduces a minimum reflection-diffraction period given by

$$(t_d - t_a)_{min} = \frac{2R}{a_{bs}} \tag{3.6}$$

Having defined the times associated with the cylinder loading time history, the only remaining variables to be defined are the pressures at times t_a and t_d, the pressure being constant for $t \geq t_d$ due to the assumption of a blast wave of infinite duration. From Ref. 5, the loading at time t_a is

$$p(t_a, \theta) = \begin{cases} \Delta p_s \bar{r}_p & , \ 0 \leq \theta \leq \frac{\pi}{4} \\ \Delta p_s \left[\bar{r}_p + (1-\bar{r}_p) \dfrac{\theta - \frac{\pi}{4}}{\frac{\pi}{4}} \right] & , \ \frac{\pi}{4} < \theta \leq \frac{\pi}{2} \\ \Delta p_s \left[1.5 - \dfrac{\theta}{\pi} \right] & , \ \frac{\pi}{2} < \theta \leq \pi \end{cases} \tag{3.7}$$

where $\bar{r}_p$ is the reflection factor for normal reflection of a shock wave,

$$\bar{r}_p = 2\left(\frac{7+4\xi}{7+\xi}\right) \tag{3.8}$$

Finally, the pressure loading at time t_d may be found from Ref. 5 as

$$p(t_d,\theta) = \Delta p_s + C_p q \tag{3.9}$$

where

C_p is a pressure coefficient

q is the dynamic pressure behind the shock front

The pressure coefficient is represented in Ref. 5 as

$$C_p = \begin{cases} 1-4\sin^2\theta & , \ 0 \leq \theta \leq \frac{\pi}{2} \\ -10.278 + 4.633\theta & , \ \frac{\pi}{2} < \theta < \frac{2\pi}{3} \\ -0.574 & , \ \frac{2\pi}{3} \leq \theta \leq \pi \end{cases} \tag{3.10}$$

The dynamic pressure may be expressed in terms of the shock strength, by using the Rankine-Hugoniot relations, as

$$\frac{q}{\frac{1}{2}\rho_o c_o^{\ 2}} = \frac{25\xi^2}{7(7+\xi)} \tag{3.11}$$

where ρ_o is the ambient density.

This completes the definition of the pressure loading on a cylinder as utilized in both the structural model response analysis and the vulnerability code.

3.4.2 Loading for Beams and Plates

The considerations which led to the use of the actual side-on loading for cylinders are not valid when beams and plates are addressed. For example, the duration of the reflection-diffraction period is a function of the size of the structure of which the beam is a part, and this size is not defined by the size of the beam. The problem of defining the pressure loading for blast-wave durations which are not long in

comparison with the reflection-diffraction period remains; however, the beam may have a long enough response time constant so that the peak response may occur well after the reflection-diffraction period. Hence, the assumption of an infinite duration blast wave is not viable for beams and plates.

Accordingly, the loading time history used for the structural model response analyses to establish the pressure-impulse curves was a simple exponential form,

$$p(t) = p_M \left(1 - \frac{t}{t_o}\right) e^{-\frac{t}{t_o}} \tag{3.12}$$

where p_M and t_o are pressure and time parameters which permit different values of pressure and impulse to be examined. The time history given by Eq. (3.12) is similar to that which will actually be encountered, in that it jumps to its peak at time zero and subsequently decays in an exponential fashion. For the pressure-impulse method to work, it is important that the loading time history on which the P-I curves are based be similar to the loading time histories for which the P-I curves will be used.

For the vulnerability code, the shock front is assumed to encounter the structure side on; that is, with the face of the structure containing the beam or panel oriented parallel to the shock front. This is at least close to being the most critical orientation. The vulnerability code then has imbedded in it a model for the side-on blast-wave loading of a flat (or nearly flat) structure. This model is taken from Ref. 6.

The pressure loading at time zero is the same as that on a cylinder at $\theta=0$; that is, from Eq. (3.7)

$$p(0) = \Delta p_s \bar{r}_p \tag{3.13}$$

where $\bar{r}_p$ is given by Eq. (3.8). To define the reflection-diffraction period, two distances, SS and S are defined in Ref. 6. The first, SS, is the distance from the point in question (taken here to be the center of the beam or plate) to the nearest free edge. A free edge as used here is represented by a position on the structure at which the structure is perpendicular to the shock wave. For example, in the case in which the front face of a box structure on the ground is being examined, the intersections of the roof and side walls with the front face would be free edges. The distance SS is used to define the time at which diffraction effects begin, t_{ss}.

Ref. 6. Dunn, B.J., Lavagnino, A., and White, J.J., Parametric Analysis of Nuclear Weapon Air Blast Effects on a Model Target, BDM/W-74-009TR, Braddock, Dunn and McDonald, Inc., December 1973.

$$t_{ss} = \frac{SS}{V_s} \tag{3.14}$$

where V_s, the shock velocity, is given by Eq. (3.3).

The second distance defined in Ref. 6, S, is the longest distance from any point on the face of the structure being considered to the farthest free edge. The distance S is used to define the time at which diffraction effects end, t_s.

$$t_s = t_{ss} + \frac{2S}{V_s} \tag{3.15}$$

From time zero to time t_{ss}, the loading will be taken to be linear. In accordance with Ref. 6, the loading at time t_{ss} is

$$p(t_{ss}) = \bar{r}_p \Delta p(t_{ss}) \tag{3.16}$$

where $\Delta p(t)$ is the overpressure associated with the blast wave at time t. It is seen that the decay in loading from time zero to time t_{ss} is due to blast wave decay rather than to diffraction effects.

From time t_{ss} to time t_s, diffraction effects cause the loading to diminish to the steady state pressure loading at time t_s, given by

$$p(t_s) = \Delta p(t_s) + q(t_s) \tag{3.17}$$

where $q(t)$ is the dynamic pressure associated with the blast wave at time t and a drag coefficient of unity has been assumed. From time t_{ss} to time t_s, the pressure loading is taken to be linear. The form of Eq. (3,17) is applicable for any time subsequent to t_s; that is,

$$p(t) = \Delta p(t) + q(t), \quad t \geq t_s \tag{3.18}$$

Equation (3.11) expresses the dynamic pressure in terms of the shock strength, which is defined by Eq. (3.2). The relationship thus expressed between dynamic pressure and overpressure is properly valid only at the shock front; it may be used as an approximation at points behind the shock front; hence,

$$\frac{q(t)}{\frac{1}{2}\rho_o c_o^2} = \frac{25\left(\frac{\Delta p(t)}{p_o}\right)^2}{7\left(7 + \frac{\Delta p(t)}{p_o}\right)} \tag{3.19}$$

Substituting Eq. (3.19) into Eq. (3.18),

$$p(t) = \Delta p(t)\left[1 + \frac{25\ \frac{\Delta p(t)}{p_o}}{7\left(7 + \frac{\Delta p(t)}{p_o}\right)} - \frac{\frac{1}{2}\rho_o c_o^2}{p_o}\right] \tag{3.20}$$

This completes the development of the pressure loading models for plates and beams in both the structural model response analyses and the vulnerability code.

3.5 Response Damage Criteria

The structural model response or damage levels which were used as response criteria were the desired iso-damage levels selected by BRL for which P-I curves would be formulated. Three distinct damage levels were specified and these levels correspond to light, moderate, or heavy damage, respectively.

Since the response analyses required a more precise definition of response criteria than light, moderate, or heavy damage, the light damage level was specified as inelastic response strain of 3%; the heavy damage level was specified as inelastic response strain corresponding to material rupture; and the moderate damage level was specified as a response corresponding to an inelastic strain level halfway between light and heavy damage.

3.6 Methods of Response Analysis

Having described the types of structural elements requiring analysis, the model boundary conditions and materials of construction, the aerodynamic loading functions, and the response damage criteria, attention may now be given to a description of the methods of response analysis.

3.6.1 Cylinder Response Analysis

As previously indicated in Subsection 3.4, the cylinder response investigations were limited to infinite duration blast-wave loadings. Hence, no P-I data points per se were obtained in the cylinder response analyses, only pressures defined by the previously stated forcing function and corresponding to the three levels of damage criteria. The method used to analyze the response of the cylinder models was the DEPICS computer code (Ref. 7) which was developed to predict the dynamic response of multi-layered cylindrical or conical bodies undergoing large non-linear elastic or inelastic deformations.

Ref. 7. Mente, L.J., The Dynamic, Elastic-Plastic, Large Displacement Response of Buckling Sensitive Cylindrical Shells to Blast-Type Loadings, -- Part I Analytical Formulation, AMC-2-68-(T), Kaman AviDyne TR-53, Kaman Sciences Corporation, August 1968.

It had originally been anticipated that DEPICS would be run in an iterative mode to permit the program to seek the pressure which would result in a given level of response for a specific combination of the cylinder parameters. However, since DEPICS would have required a considerable amount of computer time for each iterative run desired, it was subsequently decided that it would be simpler to run DEPICS in a straight response mode to obtain a number of strain response values corresponding to selective input values of the forcing function pressure. By following this approach for each combination of cylinder parameters, it was possible to construct a number of curves relating cylinder response strain to forcing function pressure. Each individual curve was then entered consecutively with the three specified levels of inelastic strain criteria and the corresponding pressure read off.

The cylinder model configurations analyzed included length-to-diameter ratios between 1 and 3 and radius-to-thickness ratios between 50 and 300. These limits are not expected to be exceeded in actual weapon system configurations.

3.6.2 Beam Response Analyses

The beam response investigations were considerably more complicated than the cylinder analyses due to the larger number of parameters involved and, additionally, due to the fact that P-I data were being sought.

The method of analysis used to obtain beam response was a modified version of the beam option of Kaman AviDyne's blast response code, NOVA (Ref. 5). The modifications consisted of two types; first, basic modifications to the program to permit accurate calculation of stresses and strains near the clamped edge, and second, modifications designed to streamline the calculation of P-I curves.

Considering the first type of modification, as indicated in Subsection 3.3, clamped edge conditions were assumed. Comparison of results from the beam code with theoretical static elastic analyses indicated that stresses near the clamped edge were badly underpredicted, particularly for relatively thin beams. The problem arises basically due to the fact that a very high stress gradient occurs near the clamped edge, and the beam program gave insufficient definition to follow this gradient. The beam program breaks the beam down into weightless beam segments connecting discrete mass points. The spacing is usually taken to be fairly even to conserve computer time, since the integration time interval which can be used is proportional to the length of the shortest segment. It was found that the addition of many closely-spaced mass points near the clamped edge permitted accurate calculation of the static edge stresses. This procedure could not be used for dynamic analyses, however, because the aforementioned dependence of the integration time interval upon segment length would have resulted in prohibitively long computer running times. The solution to this problem involves extensive modification to the computer code so that the beam segment near the clamp is handled in a pseudo-static manner. This

approach, which is described in detail in Ref. 8, resulted in computer running times approximately two orders of magnitude less than would have been required by adding sufficient mass points while predicting virtually the same response.

The second type of modification to NOVA was aimed at streamlining the calculation of P-I curves. NOVA was originally formulated to calculate the overpressure response corresponding to a preselected range and weapon yield, and the overpressure time-history corresponding to the input range and yield was internally calculated within NOVA through the employment of a self-contained blast model. In order to obtain more definitive control over the magnitude and duration of the forcing function, NOVA was modified for the P-I analysis problem to bypass the original self-contained blast model, and the basic beam and plate forcing function time-history expressed by Eq. (3.12) was inserted into NOVA. Additionally, the program was modified to iterate on the magnitude of the forcing function to obtain a preselected response criterion corresponding to a preselected value of the forcing function duration. The previously described modifications to the original NOVA computer code ultimately resulted in a revised computer code called KADBOP, an acronym for Kaman AviDyne Dynamic response of Beams or Plates, which was specifically tailored to the requirements of the planned P-I investigations.

In order to assist the reader in understanding how the basic beam option of KADBOP was intended to be used, a brief explanation of the procedures to be followed in obtaining one beam P-I data point will be presented. First, for the particular beam material selected, a particular value of L/H is chosen. Since, as previously indicated, the input value of H was selected as unity for simplification purposes, the length of the beam between clamped supports is established and is then appropriately modeled to meet the KADBOP beam response input requirements. Next, values for the area ratios shown in Figure 3.2 are selected and the input values w_2 and w_3 calculated. The material stress-strain data and the desired three levels of response criteria are then specified in the program input. Finally, a value of t_o and an initial value of p_M for the forcing function are chosen and included in the input set. At this point, the KADBOP beam response program has all the data required and is ready to calculate beam dynamic response.

Since each point on a P-I curve defines a pressure and impulse combination corresponding to a specific level of damage or response, the program has to be run in the iterative option to determine the required pressure loads. Basically, in the iterative option of KADBOP, the program holds the input loading duration parameter, t_o, constant and adjusts the input loading force parameter, p_M, until the response matches the input response criterion. Therefore, using the input value

---

Ref. 8. NOVA-2 - A Digital Computer Program for Analyzing Nuclear Overpressure Effects on Aircraft, Prepared by Kaman AviDyne for the AFWL, KA TR-128, (to be published).

of t_o and the three levels of strain criteria, the program computes three force factors which, when multiplied by the input value of p_o, determines one pressure data point for each of the three P-I damage curves being constructed. Once the pressure data point is calculated, it is a simple matter to determine the corresponding impulse, since

$$I = \int_o^{t_o} p(t)dt. \tag{3.21}$$

This same procedure would normally be repeated for other input values of t_o until enough P-I data points are available to construct the desired P-I iso-damage curves.

The original beam option of KADBOP just described was intended to be applied to the various combinations of beam geometry parameters which had been selected as typical of the beam geometries which would probably be encountered in real weapon system configurations. The ranges of beam parameters selected for analysis were: beam length-to-depth ratios of 15 to 75; A_2/A_1 area ratios of .3 to 3.6; and A_3/A_1 area ratios of 0 to 1.5.

It was further intended that the P-I data points emerging from the KADBOP response analysis would be used to construct P-I iso-damage curves for various combinations of the specified parameters and that these curves would then be imbedded in the proposed vulnerability code as tables of discrete values. The use of the proposed vulnerability code for geometry configurations intermediate to the imbedded geometries would then have required multiple interpolations. It will subsequently be indicated in Section 4 that the proposed interpolation posed a problem and that a more accurate method was adopted for imbedding P-I data in the vulnerability code.

As can be seen from the large number of parameters selected and the further consideration of the additional parameters required for curved beams, the number of P-I data points to be calculated by the iterative procedure previously described was quite extensive when all the possible combinations of the beam parameters were considered. Consequently, as will be described in the next subsection, a method was sought which would reduce the number of computer runs required to accumulate this large mass of P-I data. Before considering this aspect of the P-I data development, however, the method of response analysis for plates should be discussed.

3.6.3 Plate Response Analysis

As indicated above, extensive modification of an existing beam program was necessary in order to permit accurate calculation of stresses and strains near the clamped boundary. Similarly, it was found that plate codes which were available could not calculate accurate edge

stresses near a clamped boundary in a practical manner. (A very recent code, reported in Ref. 8, does have this capability, but was not available in time to be used for the present program.)

One alternative method available was to use the beam code, which would give essentially the correct result for moderate to high aspect ratio plates, and to modify the beam results for application to squarish plates using results of theoretical static elastic analyses of plates. The other alternative was to use an available plate code and to recognize that the edge strains would not be accurately calculated. The decision was made in favor of the first alternative, primarily because it seemed very desirable to maintain consistency between the beam and plate results.

3.6.4 Comments on Analyses

As stated earlier, the analyses are all based on clamped boundary conditions. Although this boundary condition is probably the most appropriate one to use, the error introduced by replacing the actual boundary condition, whatever it is, by an ideal clamp is not known.

Further, the use of a clamped boundary for beams forces the analyst to consider the difficult problems associated with the very high strain gradient near the clamped boundary. Questions arise as to the validity of the analysis near the boundary when applied to an actual structure. The actual structure may be stronger than the idealized structure which was analyzed because the actual edge condition is not an ideal clamp. On the other hand, it may be weaker due to the presence of edge fastenings which result in local stress concentrations. Finally, there is the question of how to apply tensile-test rupture data to a case in which the high strain is very localized and results largely from bending rather than axial load.

The analysis methods employed are geometrically as well as materially non-linear; they are capable of predicting overall buckling of a curved beam, for example. They will not predict local crippling, such as might occur in an I-beam flange. Thus, crippling is ignored in the present work. Since crippling will weaken a beam, neglecting crippling will lead to an underprediction of damage.

3.7 P-I Curve Hyperbolic Approach

The previous subsection described the methods of analysis and computer codes which were employed to initiate the studies of the non-linear dynamic response of beams, plates, and cylinders in order to generate P-I data. As previously indicated, the cylinder analyses yielded curves of pressure versus response strain for various cylinder configuration parameters and, as such, did not require formulation of the usual P-I iso-damage curves. The beam and panel-beam analyses as described, however, do yield sets of discrete P-I data points for whatever combination of beam configuration parameters are being considered. Figure 3.4 portrays a typical light damage curve for one beam material, one specific L/H value, one specific value of A_2/A_1, and one value of

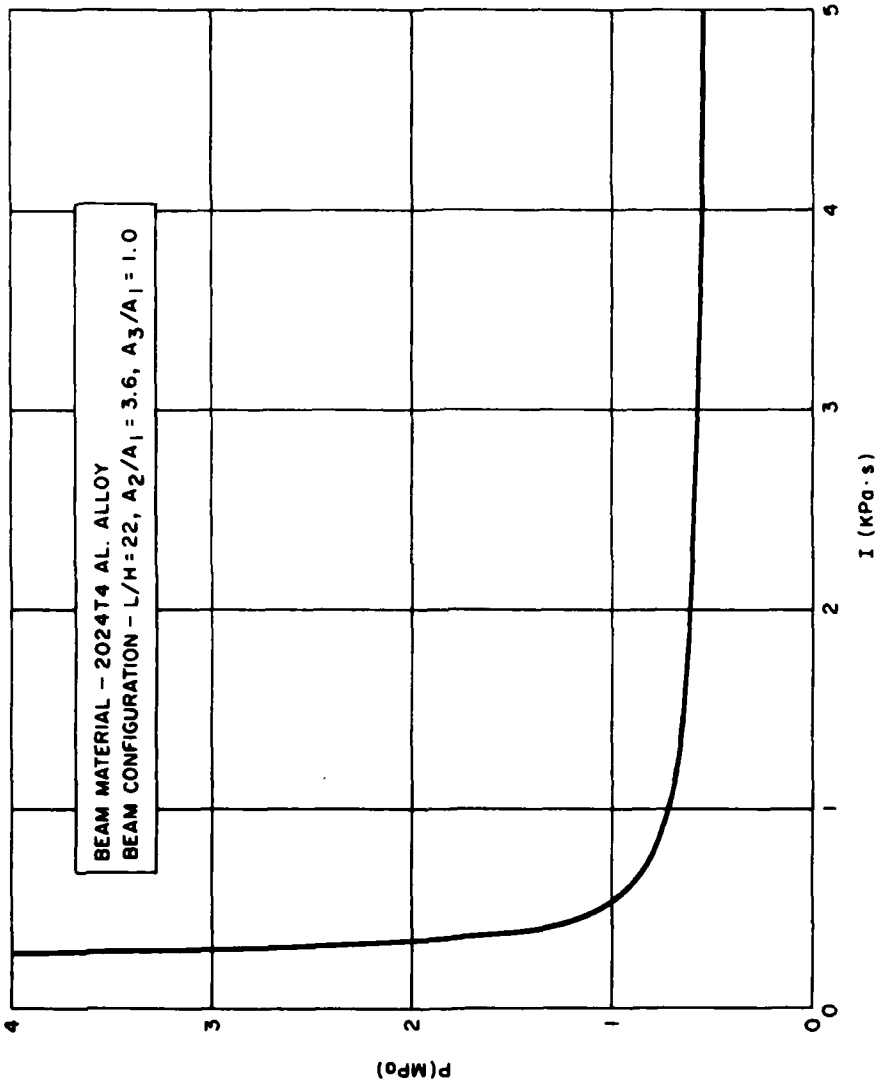

FIGURE 3.4 TYPICAL BEAM P-I CURVE

A_3/A_1. The construction of this curve represents a considerable number of discrete P-I data points and, consequently, required a considerable number of computer response runs. It rapidly became evident during the course of the beam and plate studies that the total number of required computer response runs and the attendant computer running time would reach staggering proportions in order to fulfill all the planned parametric investigations. Consequently, a method was searched for which would provide the required P-I data but with much less effort.

It has been previously recognized by other investigators that many P-I curves are hyperbolic in nature and approach asymptotic values of both pressure and impulse. On the assumption that a given P-I isodamage curve is a true hyperbola, it is possible then to take advantage of the known equation for a true hyperbola to derive several useful mathematical expressions.

The equation for a hyperbola is

$$\left(\frac{P}{P_o} - 1\right)\left(\frac{I}{I_o} - 1\right) = J \tag{3.22}$$

where P_o and I_o are the pressure and impulse asymptotes and J is a constant. The asymptotes are found by KADBOP by using a step function ($t_o \to \infty$ in Eq. (3.12)) for the pressure asymptote and by using an impulse ($t_o \to 0$, $p_M \to \infty$ in Eq. (3.12)) for the impulse asymptote. Actually, for the impulse asymptote, the initial velocity imparted to the mass points by the impulse is found and the problem is then simply an initial condition problem.

In order to determine the constant J, one more piece of information is required. The hyperbola given by Eq. (3.22) is plotted in Figure 3.5. The form is seen to be symmetric with the same scale used for both axes. The midpoint or knee point, occurs at an angle of 45° from either axis, and is designated as point K. If the pressure and impulse at point K, P_K and I_K, are defined, substitution of these values into Eq. (3.22) will allow J to be calculated. Along a 45° line on Figure 3.5, $\frac{P}{P_o} = \frac{I}{I_o}$. By integrating Eq. (3.12), the impulse is found to be

$$I = \frac{p_M t_o}{e} \tag{3.23}$$

Hence, the equation which defines the 45° line on Figure 3.5 is

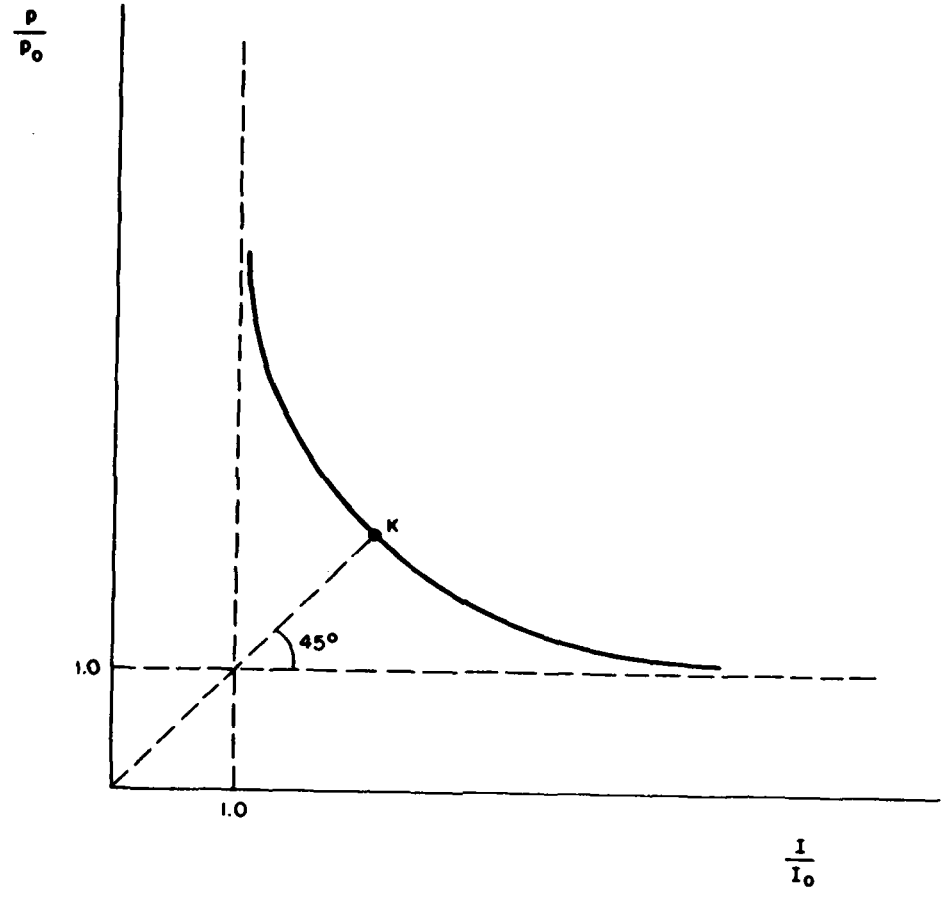

FIGURE 3.5 HYPERBOLIC REPRESENTATION OF P-I CURVE

$$\frac{p_M}{p_o} = \frac{p_M t_o^{(45)}}{eI_o}$$

or

$$t_o^{(45)} = e \frac{I_o}{P_o}$$

Thus, when P_o and I_o have been found, $t_o^{(45)}$ can be calculated. Using $t_o^{(45)}$ and an arbitary value of p_M, the response level which occurs at a point along the 45° line may be determined. By varying the value of p_M, the point at which the desired value of response occurs may be found, and the corresponding value of p_M is the value sought, P_K. The constant, J, may then be calculated as indicated.

As a check on the accuracy of the computed hyperbola, the modified KADBOP program further proceeds to calculate the response of one pair of P-I values on either side of the knee of the curve and compares these values with the strain criterion associated with the particular iso-damage curve being sought. These checks demonstrated the validity of the assumption of a hyperbolic shape for the P-I curve.

3.8 P-I Curve Usage

Suppose that at this point the analyst has available to him iso-damage curves for light, moderate, and heavy damage, and that one set of curves is for beam parameters which match a beam he wishes to analyze. The analyst may want to determine the level of response to some pressure time history, either analytically calculated or experimentally measured. He can define the peak pressure, P, and, by integration over the positive duration, the impulse, I, and can thus define a point on the P-I plane. By noting where this point falls relative to the iso-damage curves for light, moderate, and heavy damage, he can qualitatively define the desired level of response; for example, he might find that the response will be between light and moderate damage.

In Section 2, an alternative P-I approach based on work by Youngdahl in Ref. 2 and modified by Cummings and Schumacher in Ref. 3 is mentioned. Use of this approach is a bit more involved than the straight P-I approach described above. The same iso-damage curves used in the above example will be used here, and the analyst is again assumed to have a pressure time history. To implement the modified Youngdahl approach, the analyst must also select a critical pressure value, P_{cr}. Permissible values for P_{cr} in the present application range from zero to the value of the pressure asymptote for light damage. In principal, the value of P_{cr} should be related to the value of static pressure which will just produce inelastic deformation of the structure.

The analyst defines an effective impulse as

$$I_e = \int_0^{t_{cr}} p(t)dt \qquad (3.24)$$

where t_{cr} is the time at which p(t) decreases to P_{cr}. It is assumed that p(t) is of the form considered in this report; that is, starting at its maximum value and subsequently decaying in a more-or-less exponential manner. The effective pressure is then defined as

$$P_e = \frac{I_e^2}{2\int_0^{t_{cr}} tp(t)dt} \qquad (3.25)$$

The values of P_e and I_e defined using Eqs. (3.24) and (3.25) cannot be used with the P-I iso-damage curves directly. Rather, the following procedure must be used. The P-I iso-damage curves are based on the exponential loading given by Eq. (3.12), which involves the two parameters p_M and t_o. It is possible to determine the values of p_M and t_o which would yield the defined values of P_e and I_e for the given value of P_{cr}. Having p_M and t_o, the pressure, P, is immediately available as p_M and the impulse, I, is available through integration as given by Eq. (3.23). These values define a point on the P-I plane which may be used as described previously.

SECTION 4
PROCESSING DATA FOR VULNERABILITY CODE

4.1 Introduction

The previous sections have described the codes used to obtain the non-linear response of beams, panels, and cylinders. The assumption that the P-I curves are hyperbolas has been introduced and justified. At this point, then, the three data points which define a hyperbola are available for a number of beams, panels, and cylinders for three levels of response. The next task is to process these data for use in a vulnerability program.

For the cylinders, no problem exists. The number of parameters involved is so small (R/t and L/R) that numerical interpolation may be conveniently and easily used to obtain desired data for any combination of R/t and L/R within the range considered.

The situation is far different for the structures analyzed within the beam code. Here there are more parameters involved (L/H, A_2/A_1, A_3/A_1, and L/R), with the consequence that insufficient data are available to cover the parameter ranges considered in the detail required to permit reasonably accurate numerical interpolation. Hence, some means of fitting the data was sought which would be valid over the entire region.

It would be possible to establish fitting functions in a purely mathematical fashion utilizing only the available data. However, it was deemed preferable to draw upon knowledge of structural behavior to assist in arriving at appropriate fitting functions. The postulated procedure was to utilize static elastic solutions to guide the selection of fitting functions. This procedure was tried first for straight beams, with excellent results. The curved beam posed a much more challenging problem, due primarily to the snap-through phenomenon. For this reason, the fitting functions which were selected fit the straight beam data considerably better than the curved beam data.

The static elastic analysis is described in Subsection 4.2 and the reduction of the results to the straight beam case is given in Subsection 4.3. The development of the fitting functions is presented in Subsections 4.4 and 4.5 for straight and curved beams, respectively. The application of the results for 2024 Al beams to 7075 Al and to plates is described in Subsection 4.6, and the accuracy of the fitting functions is estimated in Subsection 4.7.

4.2 Static Elastic Analysis

The static elastic problem which is addressed is depicted in Figure 4.1. The curvature is assumed to be small, with the result that the axial reaction force, P, is equal to the compressive load throughout the length of the beam. The equilibrium equation is

$$EI \frac{d^2(y-y_o)}{dx^2} = -Py - M + \frac{w}{2}\left(x^2 - \frac{L^2}{4}\right) \tag{4.1}$$

where

EI is the bending stiffness
y_o defines the initial shape of the beam

and the remaining variables are defined by Figure 4.1. The initial shape is assumed to be parabolic, which is somewhat more tractable than a circular shape, leading to

$$\frac{d^2 y_o}{dx^2} = \frac{1}{R} \tag{4.2}$$

The solution of Eq. (4.1) is

$$\frac{y-y_o}{L/2} = \left[\frac{wL}{2P} - \frac{L}{2R}\right]\left[\frac{\cos\phi\bar{x} - \cos\phi}{\phi\sin\phi} - \frac{1-\bar{x}^2}{2}\right] \tag{4.3}$$

where

$$\bar{x} \equiv \frac{x}{L/2}$$

$$\phi \equiv \frac{L}{2}\sqrt{\frac{P}{EI}} \tag{4.4}$$

The solution given by Eq. (4.3) is not complete because the value of P is not known. The deformation shape defined by Eq. (4.3) may be used to determine the change in length of the beam, ΔL, and hence the average axial strain. The relationship

$$P = -EA\frac{\Delta L}{L} \tag{4.5}$$

where A is the cross-sectional area of the beam becomes, after substitution of $\frac{\Delta L}{L}$,

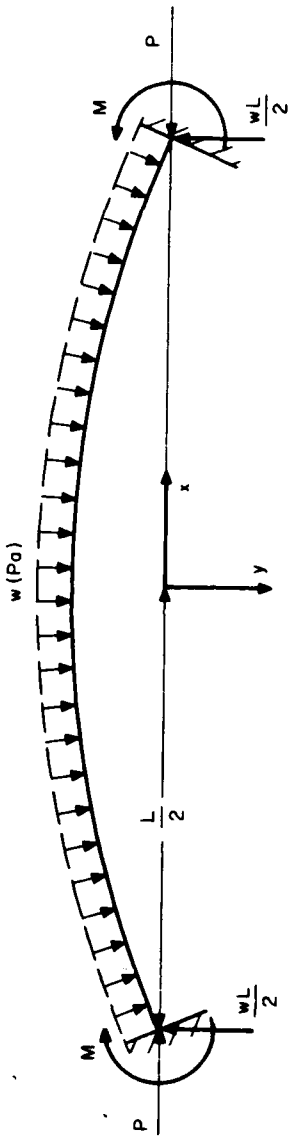

FIGURE 4.1 LAYOUT FOR STATIC BEAM ANALYSIS

$$W^2 a(\phi) + W\mu c(\phi) + \mu^2 e(\phi) = -1 \tag{4.6}$$

where

$$W \equiv \frac{wL}{AE}\eta^3 \tag{4.7}$$

$$\eta \equiv \sqrt{\frac{AL^2}{12I}} \tag{4.8}$$

$$\mu \equiv \eta\frac{L}{R} \tag{4.9}$$

and $a(\phi)$, $c(\phi)$, and $e(\phi)$ are functions of ϕ.

$$a(\phi) \equiv \frac{27}{4\phi^6}\left[\frac{1}{6} - \frac{1}{\phi^2} + \frac{1}{4\sin^2\phi} + \frac{3\cot\phi}{4\phi}\right] \tag{4.10}$$

$$c(\phi) \equiv \frac{9}{4\phi^4}\left[\frac{1}{\phi^2} - \frac{1}{2\sin^2\phi} - \frac{\cot\phi}{2\phi}\right] \tag{4.11}$$

$$e(\phi) \equiv \frac{3}{4\phi^2}\left[-\frac{1}{6} + \frac{1}{4\sin^2\phi} - \frac{\cot\phi}{4\phi}\right] \tag{4.12}$$

In arriving at this result, power series in $\left(\frac{L}{R}\right)^2$ have been truncated; for example,

$$a(\phi) = a_1(\phi) + \left(\frac{L}{R}\right)^2 a_2(\phi) + \ldots\ldots$$

has been truncated, retaining only the first term, which is consistent with the assumption of small curvature.

As $\phi \to 0$, the above expressions lose numerical accuracy badly. For small values of ϕ, the following expressions should be used.

$$a(\phi) \approx \frac{1}{140\phi^2} + 0.00143, \quad \phi \leq 0.2 \tag{4.13}$$

$$c(\phi) \approx -\frac{1}{20\phi^2} - \frac{1}{105}, \quad \phi \leq 0.2 \tag{4.14}$$

$$e(\phi) \approx \frac{1}{60} + \frac{\phi^2}{420}, \quad \phi \leq 0.2 \tag{4.15}$$

By defining

$$\omega \equiv \frac{W}{\mu} \tag{4.16}$$

Eq. (4.6) becomes

$$\omega^2 a(\phi) + \omega c(\phi) + e(\phi) + \frac{1}{\mu^2} = 0 \tag{4.17}$$

Also, substitution of the various definitions into Eq. (4.3) yields

$$\frac{y-y_o}{L/2} = \frac{L}{2R}\left[\frac{3\omega}{\phi^2} - 1\right]\left[\frac{\cos\phi\bar{x} - \cos\phi}{\phi\sin\phi} - \frac{1-\bar{x}^2}{2}\right] \tag{4.18}$$

The solution is then represented by Eqs. (4.17) and (4.18). Equation (4.17) must be solved by trial and error. First, a trial value of ϕ is assumed. (This is equivalent to selecting a trial value of P, since, for a given beam, ϕ is known once P is known.) The parameter ω may then be found from Eq. (4.17). Two values will be found, in general, since Eq. (4.17) is quadratic. For a given value of ω, the corresponding loading, w, may be found using Eqs. (4.16) and (4.7 - 4.9). If the value of w so calculated corresponds to the actual loading, a solution point has been found; otherwise, a new trial ϕ must be selected. Once convergence has been obtained, substitution of ω and ϕ into Eq. (4.18) provides the deformation shape.

The character of the solution is shown by Figure 4.2, which plots the deformation at the center of the beam, $\left[\frac{y-y_o}{-y_o}\right]_{\bar{x}=0}$, vs the loading parameter, ω. In considering Figure 4.2, remember that, for a given beam, ω is directly proportional to the loading, w, and ϕ^2 is proportional to the compressive axial load, P.

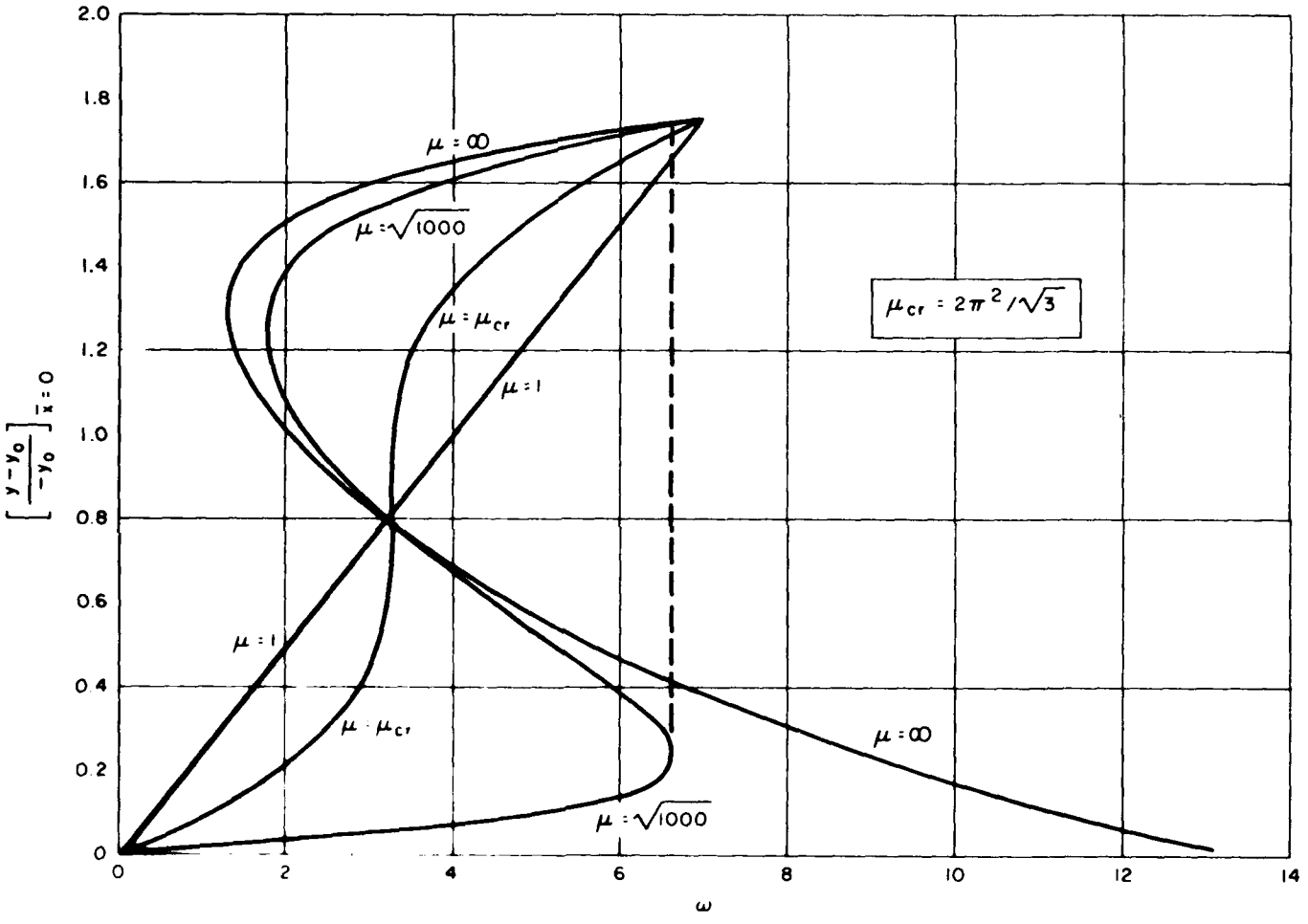

FIGURE 4 2 DEFLECTION BEHAVIOR OF CURVED BEAMS

Four curves are shown in Figure 4.2, corresponding to four different values of μ. For any value of μ, $\phi=0$ gives $\omega=0$ and $\omega=7$; hence, the ends of the curves fall at these two values of ω. Consider first the curve for $\mu=1$, a very small value of μ corresponding to a nearly straight beam. As ϕ is increased from zero, the two values of ω found for each value of ϕ move from the initial values, 0 and 7, toward each other, and meet at a small value of ϕ. Higher values of ϕ would give a complex solution for ω. For small values of μ, the normalized deflection is essentially linear with loading.

Next consider the deflection behavior for a moderately large value of μ, $\mu=\sqrt{1000}$. As ϕ increases from zero, the two values of ω approach one another, and are equal at $\phi=\pi$. The value of ω corresponding to $\phi=\pi$ is $\omega=\pi^2/3=3.290$. As ϕ increases beyond π, the two branches behave as shown, eventually converging at a point slightly above the lower knee of a value of ϕ of a little over 5. Having established the curve, consider the structural behavior as the loading parameter, ω, increases. Starting at $\omega=0$, the axial force parameter, ϕ, is zero. As ω increases, the deflection increases and so does ϕ. When ω reaches the critical value defined by the lower knee, a further increase in ω must be accompanied by a jump in deflection, as shown by the dashed line. At the same time, there is a step decrease in ϕ. This is the snap-through phenomenon. At the lower knee, the deflection pattern leaves the center of the beam above the chord joining the two ends of the beam; at the end of snap-through, the center of the beam is well below this chord.

Curves for two other values of μ are also shown in Figure 4.2. The first, for $\mu=\infty$, exhibits the same general behavior as the curve for $\mu=\sqrt{1000}$. In this case, however, there is no deflection until the snap-through load, $4\pi^2/3$, is reached.

The final curve is for $\mu = 2\pi^2/\sqrt{3}$, which is the critical value of μ, μ_{cr}. For $\mu<\mu_{cr}$, snap-through does not occur (that is, the curve is single-valued for all values of ω); for $\mu>\mu_{cr}$, snap-through does occur. For $\mu=\mu_{cr}$, the maximum value of ϕ is $\phi=\pi$.

Next consider the behavior of the beam beyond the terminal point of the upper branch on Figure 4.2. As the terminal point is approached, ϕ is decreasing and reaches zero at the terminal point. This means that the compressive axial load decreases to zero at the terminal point. For higher loadings and deflections, the axial load becomes negative; that is, the axial load becomes tensile. The loading parameter, ϕ, then becomes imaginary, as may be seen from Eq. (4.4). For convenience, the loading parameter ζ is used in the tensile regime, where

$$\phi = i\zeta \tag{4.19}$$

Referring again to Figure 4.2, the following types of elastic behavior are possible:

1) $\mu < \mu_{cr}$

Snap-through does not occur

2) $\mu > \mu_{cr}$

a) ω at snap-through <7

Beam snaps through into compression regime

b) ω at snap-through >7

Beam snaps through into tension regime

In order to interpret beam response in terms of damage, stresses must be found. Since the deformation shape has been determined, this may easily be accomplished, resulting in

$$\eta^2 \frac{\sigma}{E} = -\frac{\phi^2}{3} + \frac{\mu\chi}{2} \left| (1-\phi\cot\phi) \left(\frac{3\omega}{\phi^2} - 1\right) \right| \tag{4.20}$$

for a compressive axial force and

$$\eta^2 \frac{\sigma}{E} = \frac{\zeta^2}{3} + \frac{\mu\chi}{2} \left| (\zeta\coth\zeta - 1) \left(\frac{3\omega}{\zeta^2} - 1\right) \right| \tag{4.21}$$

for a tensile axial force, where

$$\chi \equiv \frac{2c}{L} \eta \tag{4.22}$$

Here c is the distance from the beam neutral axis to the outer fiber on the loaded side of the beam. The stresses given by Eqs. (4.20) and (4.21) are those which occur at the clamped support and are the maximum stresses which occur. In addition, Eqs. (4.20) and (4.21) are chosen to provide the tensile stresses at the support, rather than the compressive stresses, since the vulnerability program will be directed toward tensile failure. In passing, it is noted that the stress which occurs when the axial stress switches from compression to tension is

$$\left(\frac{\sigma}{c} \eta^2\right)_{\phi=0, \text{ upper branch}} = 3.5\mu\chi \tag{4.23}$$

The parameters η and χ which have been defined in the present subsection are functions of the beam cross-section. Some insight into what the parameters represent is attained by noting that for a solid cross-section η is the beam length to thickness ratio and χ is unity.

4.3 Straight Beam Results

Reduction of the curved-beam solution of the foregoing subsection to the straight-beam case is fairly straightforward. Substituting $\mu=0$ into Eq. (4.6) and recognizing that the axial force will always be tensile for a straight beam,

$$W = \sqrt{-1/a(\zeta)} \tag{4.24}$$

where

$$a(\zeta) = -\frac{27}{4\zeta^6}\left[\frac{1}{6} - \frac{1}{\zeta^2} - \frac{1}{4\sinh^2\zeta} - \frac{3\coth\zeta}{4\zeta}\right], \quad \zeta>0.2 \tag{4.25}$$

$$a(\zeta) = -\frac{1}{140\zeta^2} + 0.00143, \quad \zeta\leq 0.2 \tag{4.26}$$

The stress relation for the straight beam may be derived from Eq. (4.21) as

$$\eta^2 \frac{\sigma}{E} = \frac{\zeta^2}{3} + \frac{3\chi}{2}\frac{\zeta\coth\zeta-1}{\zeta^2} W \tag{4.27}$$

4.4 Fitting Functions for 2024 Al Straight-Beam Data

As indicated in Subsection 4.1, the straight-beam data were fitted first, and adjustments were made to the straight-beam fits to accommodate the curved beams. Futhermore, for the straight beams, the light damage data were fitted first, since it seemed likely that guidance provided by the static elastic solution would be most appropriate for the light-damage case. Hence, the straight-beam fitting functions for light damage are presented first.

4.4.1 Light Damage Fitting Functions

The relevant static result is Eq. (4.27), which must be solved together with Eqs. (4.24) and (4.25) or (4.26). Equation (4.27) yields the elastic strain resulting from the application of a static, uniform pressure. If a step-function pressure (corresponding to the pressure asymptote on the P-I hyperbola) were applied to the structure, a dynamic overstress factor would be expected compared with the stress or strain obtained by static application of the same pressure. Hence, one might expect that Eq. (4.27) would apply approximately for a step-function

pressure if a dynamic factor (really, the inverse of the dynamic factor) were applied to the left-hand side of Eq. (4.27). This was attempted, and it was found that excellent correlation with the computer results could be obtained by making this factor a function of χ. The modified version of Eq. (4.27) used to solve for the pressure asymptote thus becomes

$$\eta^2 s(\chi) = \frac{\zeta^2}{3} + \frac{3\chi}{2} \frac{\zeta \coth\zeta - 1}{\zeta^2} W \tag{4.28}$$

Solution of this equation in conjunction with Eqs. (4.24) and (4.25) or (4.26) gives the pressure asymptote, P_o. The function $s(\chi)$ is plotted in Fig. 4.3.

Having successfully fitted the P_o data, attention is next focused on the impulse asymptote, I_o. The approach used is to relate the impulse to the work done by the application of P_o, which is given by

$$\text{Work} = P_o \int_{-\frac{L}{2}}^{\frac{L}{2}} y \, dx$$

$$= P_o \left[\frac{P_o L^5}{EI} f(\zeta) \right] \tag{4.29}$$

where $f(\zeta)$ is a function of ζ which results from the indicated integration.

The kinetic energy imparted by the impulse is

$$KE = \frac{1}{2} \rho A L V^2 \tag{4.30}$$

where V is the velocity resulting from the impulse and is given by

$$V = \frac{I_o}{\rho A} \tag{4.31}$$

Substituting Eq. (4.31) into Eq. (4.30) and equating the kinetic energy imparted by the impulse to the work done by P_o,

$$\frac{I_o^2}{\rho A} = \frac{2 P_o^2 L^4}{EI} f(\zeta) \tag{4.32}$$

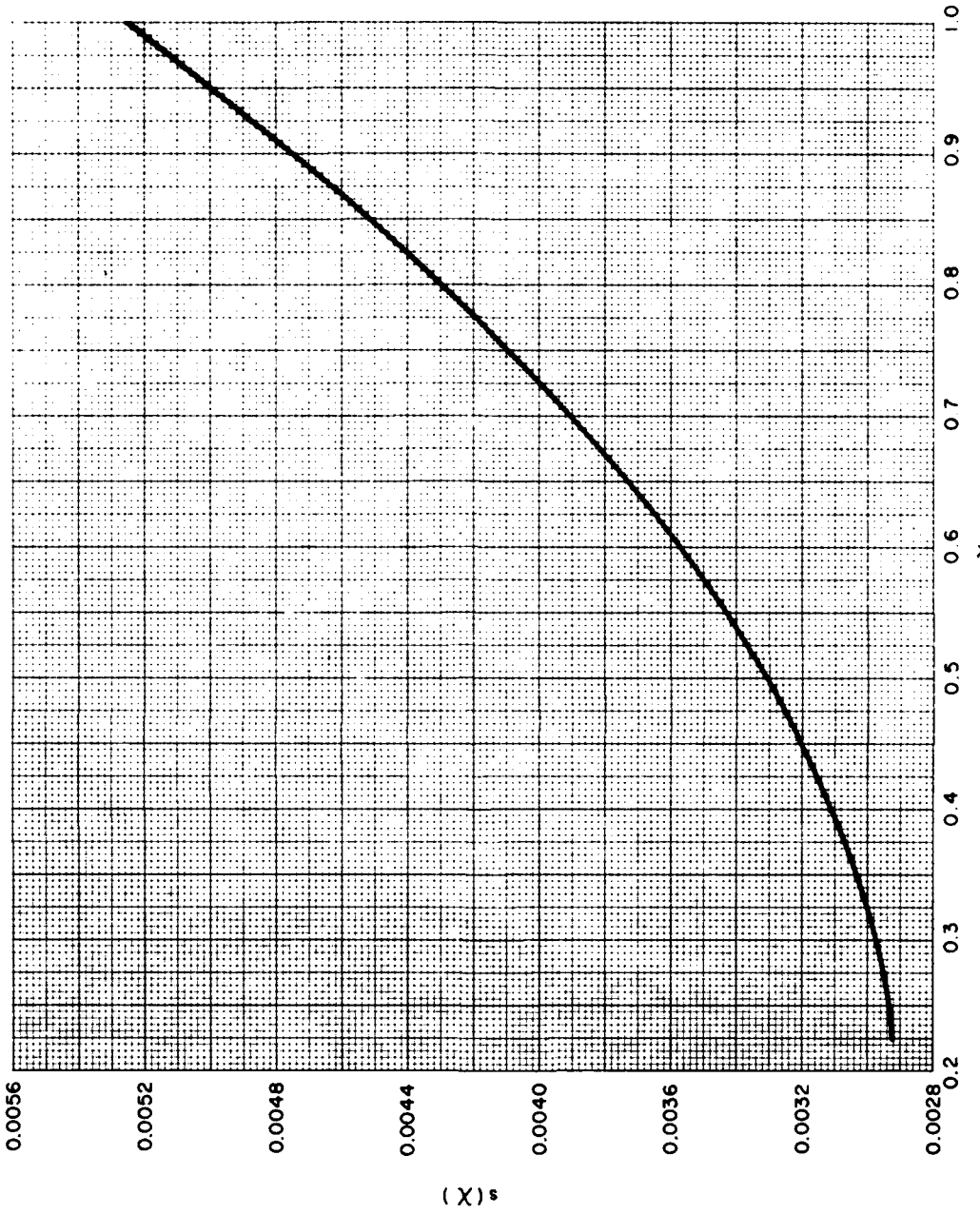

FIGURE 4.3 s(X) VS X

Introducing ζ as defined by Eq. (4.8), and defining W_o consistently with Eq. (4.7) as

$$W_o \quad \frac{P_o L}{AE} \zeta \tag{4.33}$$

Eq. (4.32) becomes

$$\frac{I_o}{\sqrt{\rho A^2 E}} = \quad \zeta(\zeta) \tag{4.34}$$

where $\zeta(\zeta)$ is simply a constant times the square root of $f(\zeta)$. Equation (4.34) may be used to find I_o; however, it was found that better correlation with the computer data was obtained by introducing a function of the parameter $2c/t$.

$$\frac{I_o}{\sqrt{\rho A^2 E}} = \frac{W_o}{\eta^2} \alpha\left(\frac{2c}{t}\right) \delta(\bar{\zeta}) \tag{4.35}$$

where

$$\alpha\left(\frac{2c}{t}\right) \equiv 1.71 - .71 \frac{2c}{t} \tag{4.36}$$

and $\delta(\bar{\zeta})$ is plotted in Figure 4.4. The parameter ζ is the value of ζ corresponding to the solution of Eq. (4.28). It should be noted that $\delta(\bar{\zeta})$ was actually determined empirically from the computer data rather than through integration of the deformation shape.

The final step is to establish a fitting function for the constant J in Eq. (3.22). It may be noted in passing that accurate fitting of J is not nearly so critical as the fitting of P_o and I_o. For example, at the knee (defined by $\frac{P}{P_o} = \frac{I}{I_o}$)

$$\left(\frac{P_K}{P_o} - 1\right)^2 = J$$

or

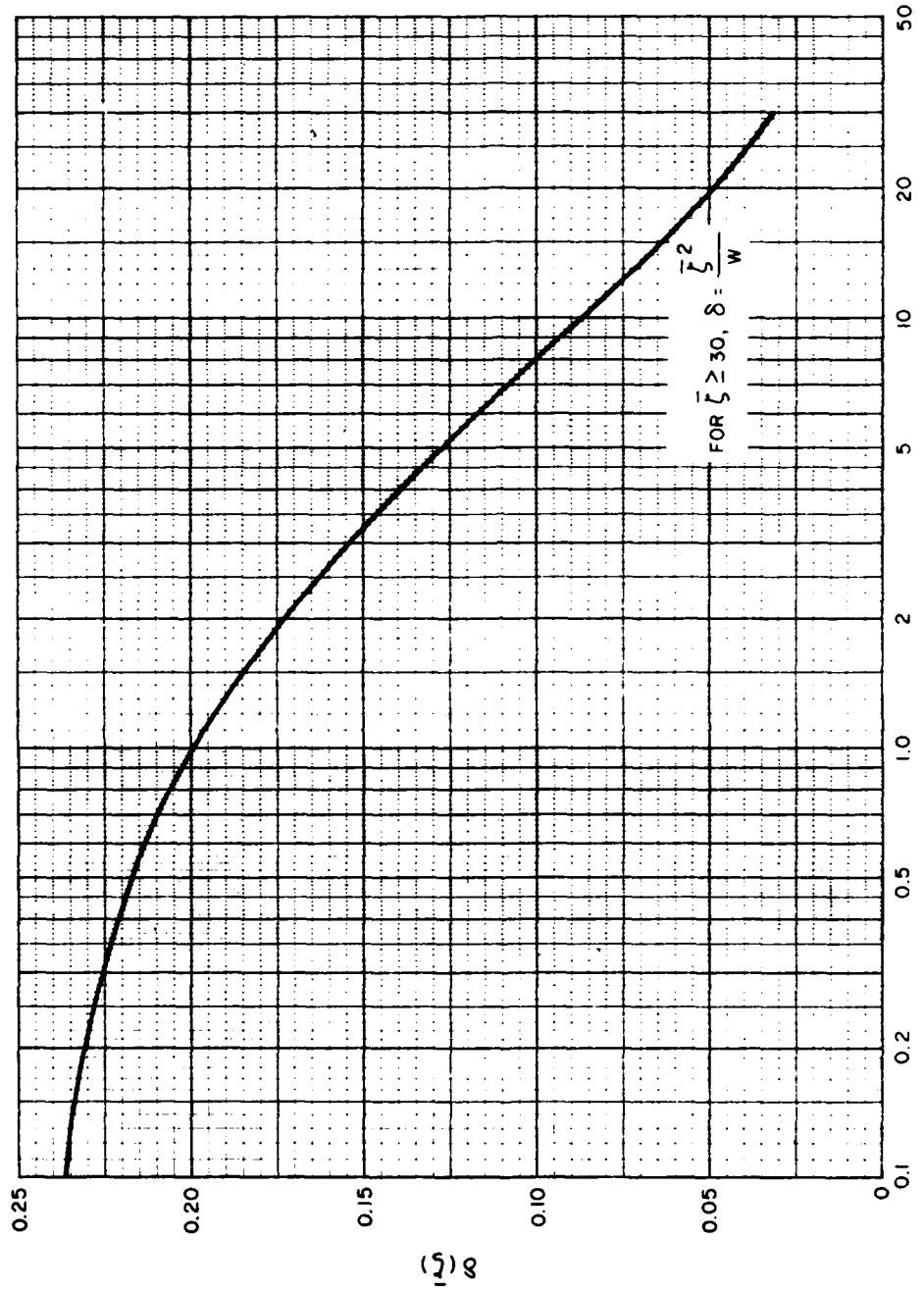

FIGURE 4.4 $\delta(\bar{\zeta})$ VS $\bar{\zeta}$

$$\frac{P_K}{P_o} = 1 + \sqrt{J}$$

The constant J falls typically in the range of 0.4 to 1.0. As an example, with J at an average value of 0.7, a fitted value of 1.0 for J, which represents over a 40% error in fitting, would result in only a 9% error in P_K.

Fitting of the constant J was done purely on the basis of the computer data, resulting in the fitting function

$$J = j(\chi)\beta(\bar{\zeta}) \tag{4.37}$$

where

$$j(\chi) \cong 0.57 + 0.52\chi \tag{4.38}$$

and $\beta(\bar{\zeta})$ is plotted in Figure 4.5.

4.4.2 Moderate and Heavy Damage Fitting Functions

The procedure used to fit the computer data for moderate and heavy damage was to build on the fitting functions for light damage. The factors used to convert the light damage factors to moderate and heavy damage factors were derived empirically from the computer data. It was found that factors could be based upon $\bar{\zeta}$, which, as indicated earlier, is the value of ζ corresponding to the solution of Eq. (4.28) for light damage. Figure 4.6 defines the ratios $\frac{P_{o_2}}{P_{o_1}}$ and $\frac{P_{o_3}}{P_{o_1}}$, which are the ratios of P_o for moderate and heavy damage, respectively, to the value of P_o for light damage. Figure 4.7 presents similar results for the impulse asymptote, I_o.

For the constant J, Eqs. (4.37) and (4.38) are used, but $\beta(\bar{\zeta})$ is redefined in Figure 4.8 for moderate and heavy damage.

4.5 Fitting Functions for 2024 Al Curved-Beam Data

As pointed out earlier, the presence of the snap-through phenomenon greatly complicates the curved-beam solution in comparison with the straight-beam solution. Using the analysis in Subsection 4.1, the static value of ω which produces snap-through can be calculated. This value of ω will be designated by ω_{ST}^{s}, where the subscript indicates snap-through and the superscript denotes static. Also, using Eqs.

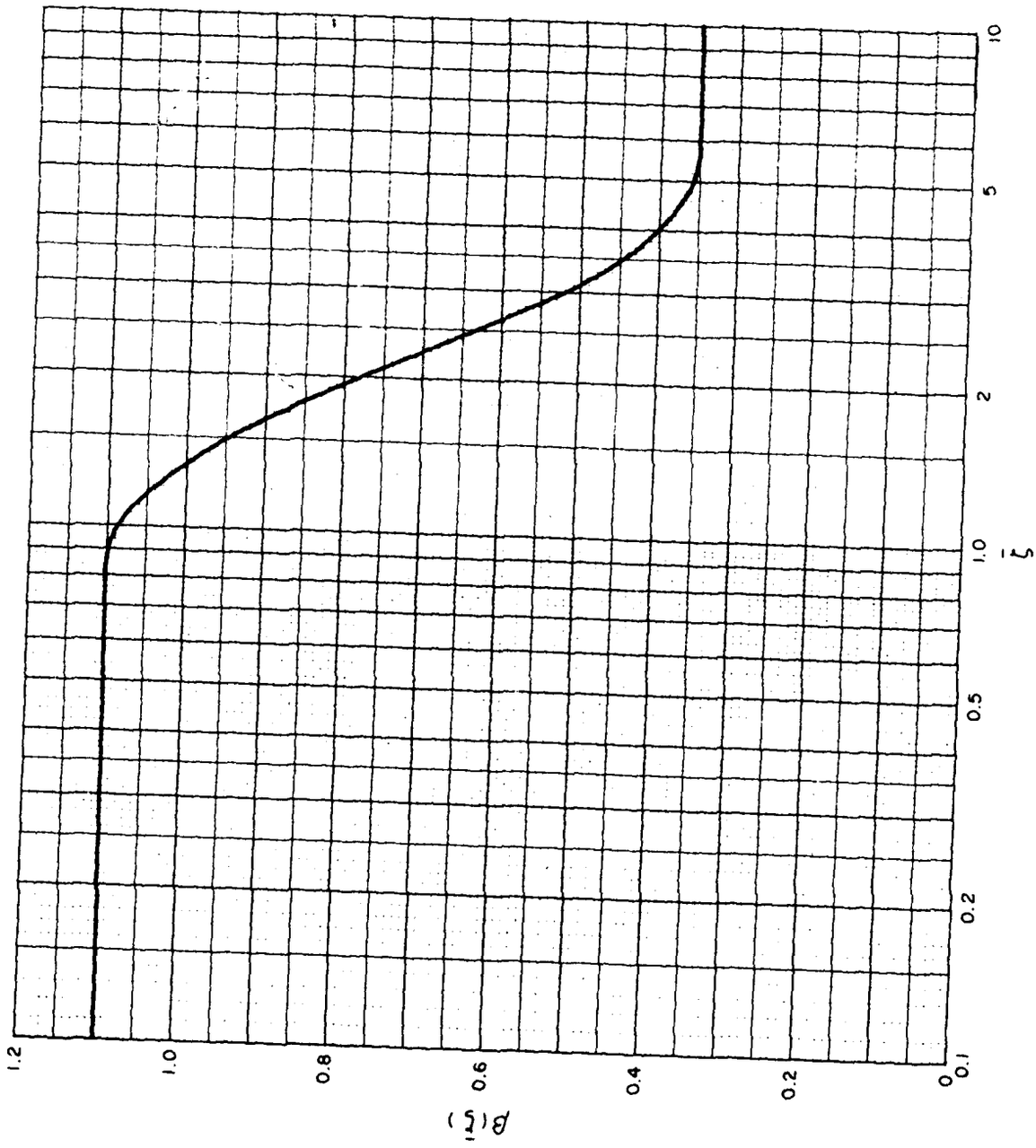

FIGURE 4.5 $\beta(\bar{\zeta})$ VS $\bar{\zeta}$ FOR LIGHT DAMAGE

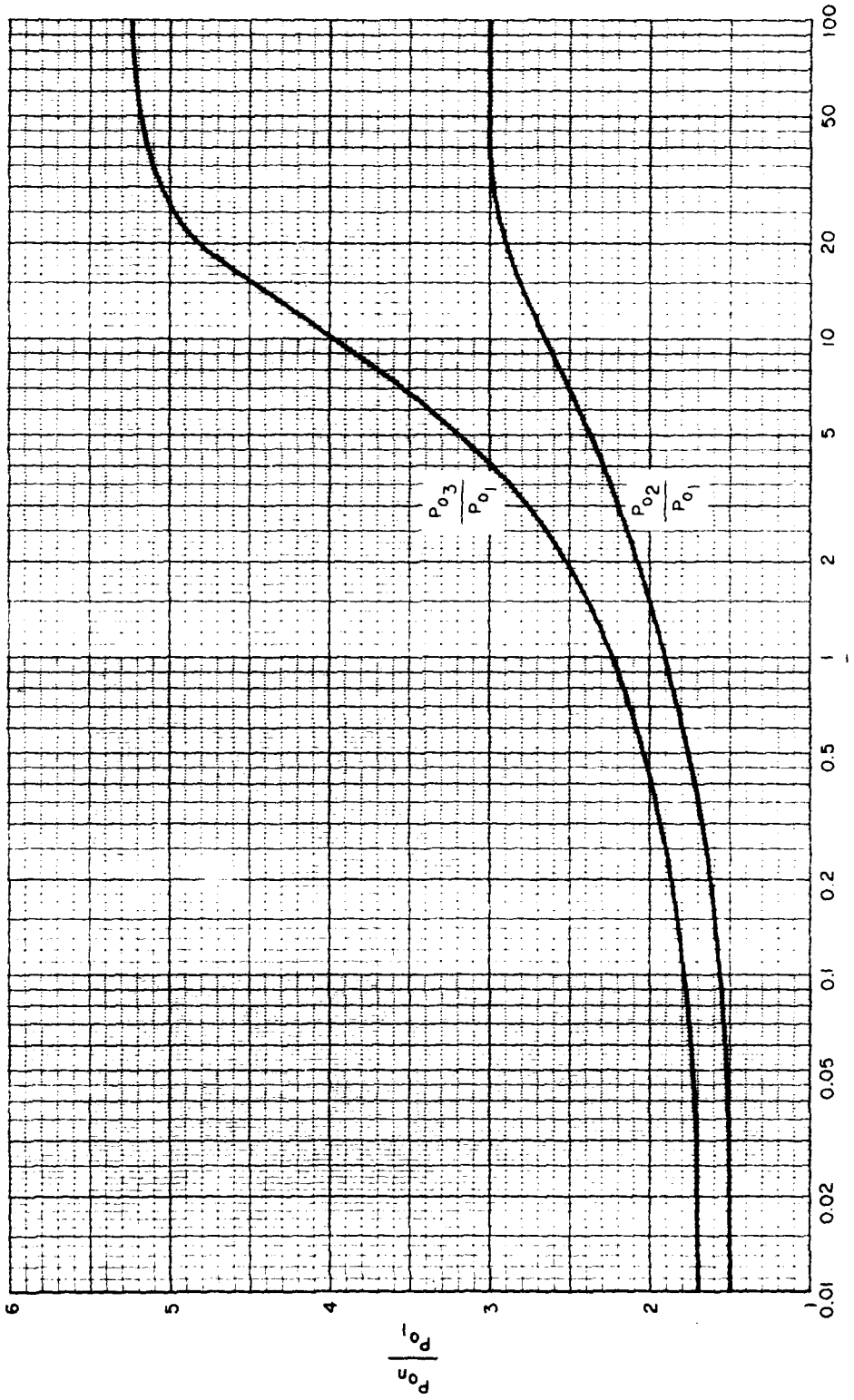

FIGURE 4.6 $\frac{P_{0n}}{P_{01}}$ VS $\bar{\zeta}$

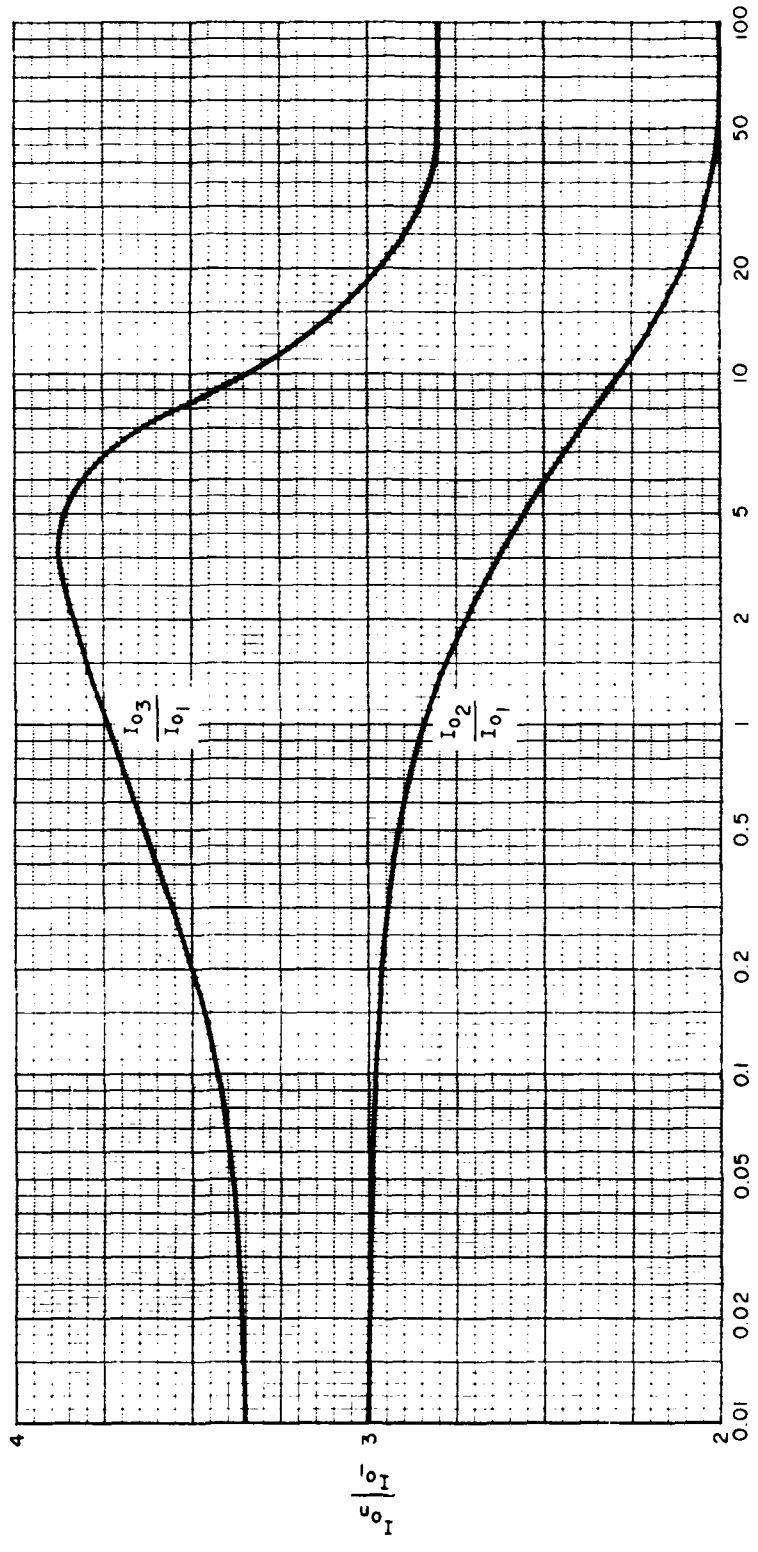

FIGURE 4.7 $\frac{I_{o_n}}{I_{o_1}}$ VS $\bar{\zeta}$

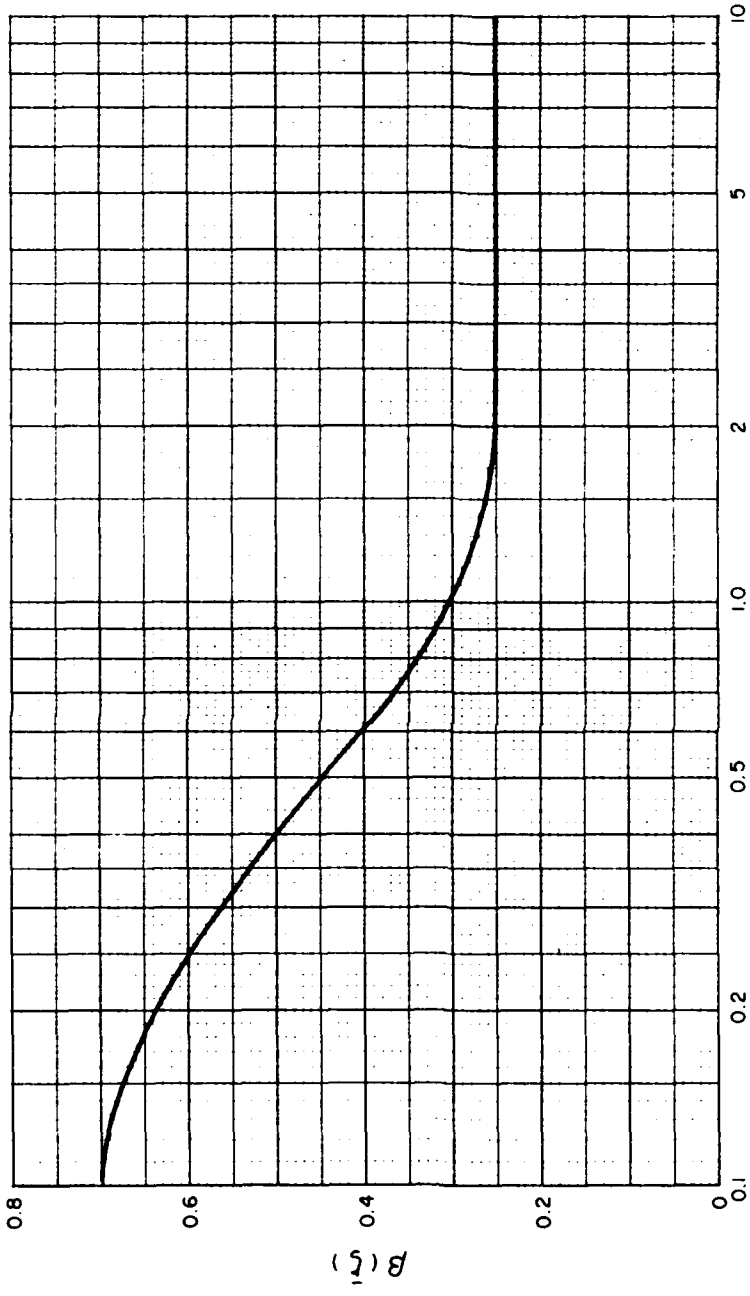

FIGURE 4.8 $\beta(\bar{\zeta})$ VS $\bar{\zeta}$ FOR MODERATE AND HEAVY DAMAGE

(4.20) and (4.21), the values of $\eta^2 \frac{\sigma}{E}$ just before and just after snap-through can be established. These will be designated by SN2B and SN2A, respectively where the notation SN2 is used to repalce $\eta^2 \frac{\sigma}{E}$ and the B and A indicate before and after snap-through.

In some cases, stress or strain, rather than snap-through, will be the dominant factor. From the straight-beam fitting functions, the parameter $s(\chi)$ is available which defines an effective value of $\frac{\sigma}{E}$. The quantity $\eta^2 s(\chi)$ will be denoted by SN2. The static value of ω will be denoted by ω_σ^s, where the subscript indicates that ω is based upon stress considerations.

In many cases, SN2 will occur in the snap-through region; that is, SN2B$\leq$SN2$\leq$SN2A. In such cases, ω_σ^s will be set equal to ω_{ST}^s.

If $\mu<\mu_{cr}$, there is no snap-through and hence ω_{ST}^s will be undefined. In the procedure to be used for fitting the curved beam data, this situation would lead to discontinuities in the solution. To avoid such discontinuities, an effective snap-through loading, ω, is defined as follows. The maximum value of the axial load parameter, ϕ, is found. From Subsection 4.2, it is known that $\phi_{max}<\pi$ for $\mu<\mu_{cr}$. Corresponding to ϕ_{max} are a value of ω, which is taken as ω_{ST}^s, and a value of $\eta^2 \frac{\sigma}{E}$, which is used to define both SN2B and SN2A.

4.5.1 Light Damage Fitting Functions

The various parameters developed in the previous section are used to define the light damage fitting functions. In fitting P_o, there are two main cases; $\omega_\sigma^s < \omega_{ST}^s$ and $\omega_\sigma^s \geq \omega_{ST}^s$. These two cases are examined below.

Case 1: $\omega_\sigma^s < \omega_{ST}^s$

The desired value of ω, from which P_o can be calculated, is the smaller of ω_σ^D or ω_{ST}^D, where the superscript denotes dynamic and

$$\frac{\omega_\sigma^D}{\omega_\sigma^s} \equiv \begin{cases} 1.0, & \frac{L}{R} \leq 0.4 \\ 1.0-0.45\left(\frac{L}{R} - 0.4\right), & \frac{L}{R} > 0.4 \end{cases} \tag{4.39}$$

$$\frac{\omega_{ST}^D}{\omega_{ST}^s} \equiv \begin{cases} F_{ST}\left(\mu_{cr}, \frac{L}{R}\right), & \mu \leq \mu_{cr} \\ F_{ST}\left(\mu, \frac{L}{R}\right), & \mu > \mu_{cr} \end{cases} \tag{4.40}$$

In Eq. (4.40), $F_{ST}\left(\mu, \frac{L}{R}\right)$ is a snap-through factor which is plotted in Fig. 4.9. The curve for $\frac{L}{R} = 0$ is shown only to permit interpolation of F_{ST} for values of $\frac{L}{R}$ less than 0.4; it is apparent that $\mu>0$ is not compatible with $\frac{L}{R} = 0$.

In preparation for the fitting of the moderate and heavy damage computer data, SN2B is modified as follows:

$$SN2B = \begin{cases} SN2 + \dfrac{\omega_{ST}^{D} - \omega_{\sigma}^{D}}{\omega_{ST}^{s} - \omega_{\sigma}^{D}} \ (SN2B-SN2), & \omega_{ST}^{D} > \omega_{\sigma}^{D} \\ SN2 & , \ \omega_{ST}^{D} \leq \omega_{\sigma}^{D} \end{cases} \tag{4.41}$$

Case 2: $\omega_{\sigma}^{s} \leq \omega_{ST}^{s}$

For this case, the desired value of ω is approximated by

$$\omega = \begin{cases} \omega_{ST}^{D} + \left(\omega_{\sigma}^{D} - \omega_{ST}^{D}\right)\sqrt{\dfrac{\mu_{cr}}{\mu}} & , \ \mu > \mu_{cr} \\ \omega_{\sigma}^{D} & , \ \mu \leq \mu_{cr} \end{cases} \tag{4.42}$$

where

$$\frac{\omega_{\sigma}^{D}}{\omega_{\sigma}^{s}} \equiv \begin{cases} F_{ST}\left(\mu, \frac{L}{R}\right) & , \ \mu > \mu_{cr} \\ F_{ST}\left(\mu_{cr}, \frac{L}{R}\right) & , \ \mu \leq \mu_{cr} \end{cases} \tag{4.43}$$

$$\frac{\omega_{ST}^{D}}{\omega_{ST}^{s}} \equiv \begin{cases} F_{ST}\left(\mu, \frac{L}{R}\right) & , \ \mu > \mu_{cr} \\ F_{ST}\left(\mu_{cr}, \frac{L}{R}\right) & , \ \mu \leq \mu_{cr} \end{cases} \tag{4.44}$$

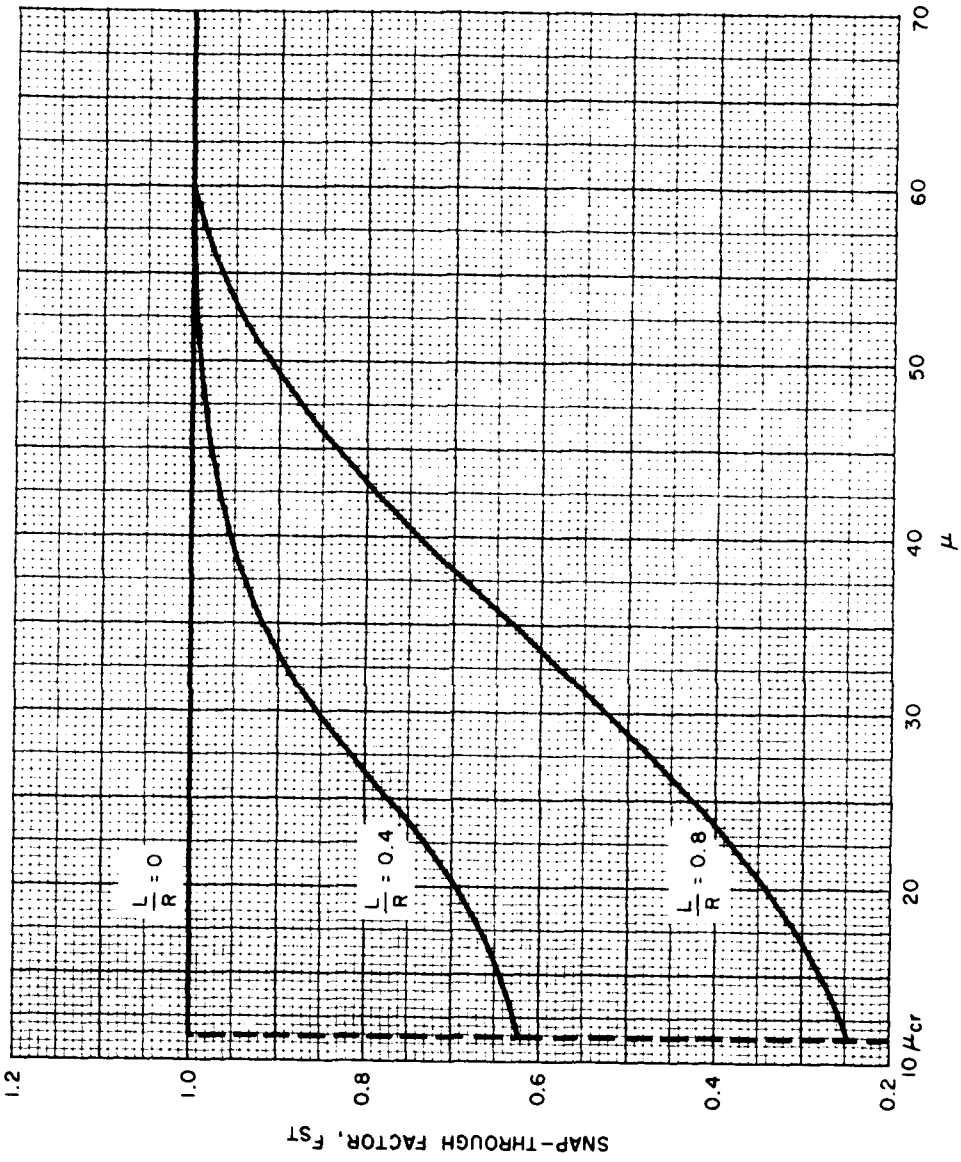

FIGURE 4.9 SNAP-THROUGH FACTOR, F_{ST}

As in the case of the straight beam, the curved-beam fitting function for the impulse asymptote, I_o, is based upon energy considerations. Basically, Eq. (4.35) is used for the curved beam, with two modifications. The first has to do with the deflection function, δ. It will be recalled that the value of δ used for the straight beam was that determined empirically from the computer data, rather than the value calculated by integration of the deflection shape. It is apparent that the straight-beam δ is inappropriate for curved beams. The procedure adapted was to determine δ analytically, from the deflection shape, for both the straight and curved beams. These are denoted by $\bar{\delta}(\bar{\phi})$ and $\bar{\delta}(\bar{\zeta})$, respectively, where $\bar{\phi}$ is the value of ϕ corresponding to the solution of Eq. (4.6) and $\bar{\zeta}$ is, as indicated earlier, the value of $\bar{\zeta}$ corresponding to the solution of Eq. (4.28) for the straight beam. In the case in which the curved-beam solution lies in the snap-through region, $\bar{\delta}(\bar{\phi})$ cannot be defined directly; however, the values of $\bar{\delta}$ just before and just after snap-through can be found. These will be denoted by $\bar{\delta}_B$ and $\bar{\delta}_A$, respectively. The equivalent value of $\bar{\delta}$ in the snap-through region is calculated from

$$\bar{\delta}(\bar{\phi}) = \left[\bar{\delta}_B^2 + \frac{SN2-SN2B}{SN2A-SN2B}\left(\bar{\delta}_A^2 - \bar{\delta}_B^2\right)\right]^{1/2} \tag{4.45}$$

The expression which defines $\bar{\delta}(\bar{\phi})$ based on integration of the deflection shape is

$$\bar{\delta}(\bar{\phi}) = \frac{1}{\bar{\phi}}\left[\left(\frac{3}{\bar{\phi}^2} - \frac{1}{\omega}\right)\left(1 - \bar{\phi}\cot\bar{\phi} - \frac{\bar{\phi}^2}{3}\right)\right]^{1/2} \tag{4.46}$$

Equation (4.46) is used by itself to define $\bar{\delta}$ outside of the snap-through region. In the snap-through region, Eq. (4.46) is used to define $\bar{\delta}_B$ and $\bar{\delta}_A$, and Eq. (4.45) is then used to determine $\bar{\delta}(\bar{\phi})$.

The expression for $\bar{\delta}(\bar{\zeta})$ for the straight beam is

$$\bar{\delta}(\bar{\zeta}) = \frac{1}{\bar{\zeta}^2}\left[3\left(1 - \bar{\zeta}\coth\bar{\zeta} + \frac{\bar{\zeta}^2}{3}\right)\right]^{1/2} \tag{4.47}$$

This equation is poorly behaved for small values of $\bar{\zeta}$, as is Eq. (4.46) for small values of $\bar{\phi}$. The relevant expressions for small values of $\bar{\phi}$ and $\bar{\zeta}$ are

$$\bar{\delta}(\bar{\phi}) \approx \bar{\phi}\left[\left(\frac{3}{\bar{\phi}^2} - \frac{1}{\omega}\right)\left(1 + \frac{2\bar{\phi}^2}{21}\right)\Big/45\right]^{1/2}, \quad \bar{\phi} \leq 0.3 \tag{4.48}$$

$$\bar{\delta}(\bar{\zeta}) \approx \left[\left(1 - \frac{2\bar{\zeta}^2}{21}\right)\Big/15\right]^{1/2}, \quad \bar{\zeta} \leq 0.3 \tag{4.49}$$

The modification to Eq. (4.35) to reflect the curved-beam deflection is simply to replace $\delta(\bar{\zeta})$ by $\bar{\delta}(\phi)\left[\frac{\delta(\bar{\zeta})}{\bar{\delta}(\bar{\zeta})}\right]$. It is clear that this reduces to the straight-beam result for very small curvature, since for that case $\bar{\delta}(\bar{\phi}) \sim \bar{\delta}(\bar{\zeta})$. In this connection, it must be noted that $\bar{\phi}$ for this case will be imaginary, indicating axial tension. The use of $\bar{\phi}$ instead of $i\bar{\zeta}$ or simply $\bar{\zeta}$ is retained to simplify differentiation between the curved and straight beam.

The second modification made to Eq. (4.35) involves multiplication by the factor used in Eq. (4.39). Thus, the final result is

$$\frac{I_o}{\sqrt{\rho A^2 E}} = \frac{W_o}{\eta^2}\alpha\left(\frac{2c}{t}\right)\bar{\delta}(\bar{\phi})\left[\frac{\delta(\bar{\zeta})}{\bar{\delta}(\bar{\zeta})}\right]\begin{cases} 1 & , \frac{L}{R} \leq 0.4 \\ 1-0.45\left(\frac{L}{R} - 0.4\right) & , \frac{L}{R} > 0.4 \end{cases} \tag{4.50}$$

The fitting function for the constant J involves a very simple modification of Eq. (4.37).

$$J = j(\chi)\beta(\bar{\zeta})\left(1 + \frac{L}{R}\right) \tag{4.51}$$

4.5.2 Moderate and Heavy Damage Fitting Functions

From the straight-beam solution, the parameter $\frac{P_{o_n}}{P_{o_1}}$ is available. A curved-beam pressure factor is defined as

$$PF_n \equiv 1 + \left(\frac{P_{o_n}}{P_{o_1}} - 1\right)e^{-3\frac{L}{R}} \tag{4.52}$$

From the curved-beam solution for light damage, the loading parameters $\omega^D_{o_1}$, ω^D_{ST}, and ω_1, are available, where the subscript "1" has been added to denote the first damage level, light damage. A new loading parameter is defined by

$$\bar{\omega}^D_{ST} = \begin{cases} \dfrac{SN2A}{Max(SN2,SN2B)}\ \omega^D_{ST}, & SN2A>SN2 \\ \omega^D_{ST}, & SN2A\leq SN2 \end{cases} \tag{4.53}$$

where the notation Max(a,b) signifies that the larger of "a" or b should be used. The loading range from ω^D_{ST} to $\bar{\omega}^D_{ST}$ may be considered to represent an effective dynamic loading range for snap-through. Finally, one more loading parameter is defined

$$\bar{\omega}_n \equiv \omega_1 PF_n \tag{4.54}$$

Based on the definitions given by Eqs. (4.52) - (4.54), the desired loading parameter which gives the pressure asymptote for moderate and heavy damage may be found as follows:

Case 1: $\bar{\omega}_n \leq \omega^D_{ST}$

$$\omega_n = \bar{\omega}_n \tag{4.55}$$

Case 2: $\omega^D_{ST} < \bar{\omega}_n \leq \bar{\omega}^D_{ST}$

$$\omega_n = \omega^D_{ST} \tag{4.56}$$

Case 3: $\bar{\omega}_n > \bar{\omega}^D_{ST}$

Define another intermediate loading parameter by

$$\bar{\bar{\omega}}_n \equiv \bar{\omega}_n - \bar{\omega}^D_{ST} + \omega^D_{ST} \tag{4.57}$$

Then

$$\omega_n = \begin{cases} \omega_{ST}^D + \left(\bar{\omega}_n - \omega_{ST}^D\right)\sqrt{\dfrac{\mu_{cr}}{\mu}} & , \mu > \mu_{cr} \\ \\ \bar{\omega}_n & , \mu \leq \mu_{cr} \end{cases} \tag{4.58}$$

Turning next to the impulse asymptote, use will be made of the straight-beam values of $\dfrac{P_{o_n}}{P_{o_1}}$ and $\dfrac{I_{o_n}}{I_{o_1}}$.

$$\left(\frac{I_{o_n}}{I_{o_1}}\right)_{CB} = \sqrt{\frac{\omega_n/\omega_1}{P_{o_n}/P_{o_1}}}\ \frac{I_{o_n}}{I_{o_1}} \tag{4.59}$$

where the subscript "CB" denotes curved-beam and is used to differentiate the curved-beam impulse ratio from the straight-beam impulse ratio on the right-hand side of Eq. (4.59).

Finally, the constant J for the curved beam for moderate and heavy damage is given by Eq. (4.51), with the value of $\beta(\bar{\zeta})$ selected for the appropriate damage level.

4.6 Application of Fitting Functions to 7075 Al and to Plates

The fitting functions defined thus far apply to straight and curved beams of 2024 Al. For 7075 Al beams, the pressure and impulse asymptote may be found by multiplying the 2024 Al results by the following factors; 1.4, 0.95, and 0.86 for the pressure asymptote, and 1.3, 0.71, and 0.68 for the impulse asymptote, where the three numbers apply for the three damage levels. In order to avoid situations in which, for example, $P_{o_2} < P_{o_1}$, which might occur in snap-through cases using the above numbers, P_{o_2} is taken as the larger of P_{o_1} and P_{o_2}, etc. The constant J is unchanged.

For plates, the beam results are multiplied by a function of aspect ratio, AR, where the aspect ratio is the ratio of the length of the long side of the plate to the length of the short side. The beam is effectively a plate of infinite aspect ratio. The function of aspect ratio is

$$F_{AR} = 1 + .47e^{-11(AR-1)} \qquad (4.60)$$

Both the pressure and impulse asymptotes for the beam are to be multiplied by F_{AR}. The constant J is unchanged.

4.7 Fitting Accuracy

The estimated accuracy of the fits defined in the preceding subsections is given in Table 4.1. The accuracies cited should be regarded as seldom-exceeded values; that is, in most cases the accuracy will be better than that given. The fitting functions are believed to be unbiased; that is, on the average the fitting functions will agree with the computer data. It is important to realize that the accuracies presented describe the fitting accuracy only; they do not purport to define the overall accuracy of the procedure in predicting various levels of damage for a real structure. The latter could be realistically defined only through a comprehensive testing program and/or comparison with existing test data.

TABLE 4.1

ACCURACY OF FITTING FUNCTIONS

Structural Type	Straight Beam		Curved Beam		Flat Plate		Curved Plate	
Material	2024	7075	2024	7075	2024	7075	2024	7075
Estimated Accuracy (%)	5	10	15	20	15	20	25	25

SECTION 5
PIVUL PROGRAM DESCRIPTION

5.1 Introduction

This section describes PIVUL, the Pressure-Impulse VULnerability program. The program utilizes the data from the computer runs, fitted as described in the previous section, to predict vulnerability of simple structural elements. There are four basic vulnerability options:

1. The user specifies the weapon yield, defines the structure and the desired level of damage, and the program calculates the range at which that level of damage occurs.
2. The user specifies the duration (t_o) of an exponential forcing function $\left(P = P_{MAX}\left(1 - \frac{t}{t_o}\right)e^{-\frac{t}{t_o}}\right)$, defines the structure and the desired level of damage, and the program calculates the value of P_{MAX} which produces that level of damage.
3. The user specifies the weapon yield and range and defines the structure and the program calculates the corresponding level of damage.
4. The user provides a curve of pressure vs time and defines the structure and the program calculates the level of damage.

In all cases, ambient conditions are assumed to correspond to sea level. Options 1 and 2 are solved by trial and error by the program; the solutions for Options 3 and 4 are direct.

As indicated earlier, the loading on the cylinder is assumed to be sufficiently long in comparison with the response time so that only the peak overpressure is required to define the loading. Hence, Options 2 and 4 are inapplicable for cylinders.

For plates and beams, the surface of the structure containing the plate or beam is assumed, for Options 1-3, to be oriented parallel to the shock front, since this is the most critical orientation, or at least very close to it. The loading produced by the shock reflection and subsequent diffraction waves is included in the loading calculated by the program for Options 1-3.

Subsection 5.2 contains a brief description of the various subroutines contained in PIVUL. The major program variables are defined in Subsection 5.3 and the program input is described in Subsection 5.4. Subsection 5.5 contains comments on program operation and describes the output. Finally, an example problem is given in Subsection 5.6.

5.2 Description of Subroutines

The PIVUL program is the main program which controls the flow of the overall program. PIVUL also reads the input and provides the output. PIVUL calls the following subroutines: BEAM, BLAST, CYL, PCURV, PHYP, PINT, RITER, SIDE, YOUNG and YPI.

Of the above group of subroutines, only BEAM, BLAST, and CYL call other subroutines. The order of listing the subroutines will fall into three groups below; those called by PIVUL, except for BEAM, BLAST, and CYL, the BEAM group, the BLAST group, and the CYL group. Within each group, the order will be alphabetical following the master program.

5.2.1 PIVUL Group

PCURV

Given peak pressure and duration of an exponential forcing function, calculates pressure-time points.

Called by PIVUL.

PHYP

Calculates intersection of straight line with hyperbola in P-I plane.

Called by PIVUL.

PINT

Calculates pressure and impulse from points defining pressure-time wave.

Called by PIVUL.

RITER

Controls iteration to determine critical range for option 1 or critical pressure for option 2.

Called by PIVUL.

SIDE

Calculates side-on loading from free-field pressure-time history.

Called by PIVUL.

YOUNG

Calculates effective pressure and effective impulse from points defining pressure-time curve using modified Youngdahl approach.

Called by PIVUL.

YPI

Defines the exponential forcing function which gives desired effective pressure and effective impulse and calculates associated pressure and impulse.

Called by PIVUL.

5.2.2 BEAM Group

BEAM

Master program for BEAM group. Defines P-I hyperbola for straight beams and controls flow for curved beams.

Calls BDATA, CURVB, INT1, and SNAP.

Called by PIVUL.

BDATA

Contains data defining fitting functions described in Section 4.

Called by BEAM.

CURVB

Defines P-I hyperbola for curved beams.

Calls INT1, INTERP and SETUP.

Called by BEAM.

INT1

Performs one-dimensional interpolation.

Called by BEAM and CURVE.

INTERP

Performs one-, two-, and three-dimensional interpolations.

Called by CURVB (and by CYL in CYL group).

SETUP

Sets up tables of functions of ϕ used in solving Eq. (4.17).

Called by CURVB.

SNAP

Calculates value of ω associated with snap-through and value of ω associated with the stress parameter SN2. Provides values of stress parameter before and after snap-through, and associated deflection parameters for use in defining the impulse asymptote on the P-I hyperbola.

Calls WTEN.

Called by BEAM.

WTEN

Calculates ω for solution in tension region.

Called by SNAP.

5.2.3 BLAST Group

BLAST

Calculates pressure-time points given weapon yield and range.

Calls HYPRA and WFZR.

Called by PIVUL.

HYPRA

Processes AFWL 1KT standard blast model.

Calls IOPT1, IOPT2, and IOPT3.

Called by BLAST.

IOPT1

Determines overpressure given time and range.

Calls KSHK.

Called by HYPRA.

IOPT2

Determines blast wave radius and peak overpressure given time (not used in PIVUL program).

Calls WFPKOP and WFPR.

Called by HYPRA.

IOPT3

Determines time of shock arrival and peak overpressure given range.

Calls WFPKOP and WFPR.

Called by HYPRA.

KSHK*

Calculates overpressure given time and range.

Calls WFPKOP, WFPR, WFPRMT, and WFZR.

Called by IOPT1.

WFPKOP*

Calculates peak overpressure at specified range.

Called by IOPT2, IOPT3, and KSHK.

WFPR*

Calculates blast wave radius at specified time.

Called by IOPT2 and KSHK.

*These routines are modifications of routines written by AFWL.

WFPRMT*

Calculates overpressure waveform.

Called by KSHK.

WFZR*

Calculates the range corresponding to zero overpressure at specified time.

Called by BLAST and KSHK.

5.2.4 CYL Group

CYL

Determines the critical free-field overpressure for a cylinder from tabulated data. The tabulated data are functions of R/t, L/D, and damage level.

Calls INTERP.

Called by PIVUL.

INTERP

Performs one-, two-, and three-dimensional interpolations.

Called by CYL (and by CURVB in BEAM group).

5.3 Major Program Variables

The major program variables are defined in the following list. An asterisk preceding a variable name indicates that the variable is an input variable. The dimension of the variable is also given, if applicable. Most variables are in English units, since the program works in that system. All input-output quantities are metric. Variables which are metric end in the letter M, and the following list specifically identifies metric variables.

A(629)	$a(\phi)$ for 629 values of ϕ, where $a(\phi)$ is defined in Eqs. (4.10) and (4.13)
AEL	Cross-sectional area of beam times modulus of elasticity divided by beam length
AJ(3)	Hyperbolic constants, J, for three damage levels
ALPHA	$\alpha\left(\frac{2c}{t}\right)$ defined in Eq. (4.36)
AR	Plate aspect ratio
ATOTL	Cross-section area
*ATOTM	Cross-section area, metric
BETA	Value of $\beta(\bar{\zeta})$ used to define J, Eq. (4.37)
BETAT(186)	Tabulated values of fitting function $\beta(\bar{\zeta})$ plotted in Figures 4.5 and 4.8
BI	Impulse or effective impulse from blast pulse
BIGW	Loading parameter, W, defined in Eq. (4.7)
*BLM	Beam length, metric
BLNTH	Beam length
BP	Pressure or effective pressure from blast pulse
CAE(629)	$\left[\frac{c^2(\phi)}{4a(\phi)} - e(\phi)\right]$ for 629 values of ϕ, where $a(\phi)$, $c(\phi)$ are defined in Eqs. (4.10 - 4.15)
CENTI	Cross-section moment of inertia
CHI	χ, defined in Eq. (4.22)
CHIT(31)	Values of χ used in tabulating data for $s(\chi)$ in Figure 4.3
*CLDD	Cylinder length to diameter ratio
*CLDR	Beam length to radius of curvature ratio
CLDRT(3)	Values of L/R used in tabulating data for snap-through factor plotted in Figure 4.9
CNST	Hyperbolic constant J

*CNTIM	Cross-section area moment of inertia, metric
CNTRD	Distance from neutral axis to outer fiber on loaded side
*CNTRM	Distance from neutral axis to outer fiber on loaded side, metric
CRIT(4)	Response criteria used in iteration process which drives criterion to 1.0 in CRIT(N),N=1,2,3; CRIT(4) contains convergence criterion for iteration
C2A(629)	$\frac{C(\phi)}{2a(\phi)}$ for 629 values of ϕ, where $a(\phi)$ and $c(\phi)$ are defined in Eqs. (4.10), (4.11), (4.13), and (4.14)
DBA	Deflection parameter $\bar{\delta}_A$ which appears in Eq. (4.45)
DBAR	Deflection parameter $\bar{\delta}$ defined in Eqs. (4.45) - (4.49))
DRB	Deflection parameter $\bar{\delta}_B$ which appears in Eq. (4.45)
DELT(31)	Tabulated values of fitting function $\delta(\bar{\zeta})$ plotted in Figure 4.4
DELZ	Value of $\delta(\bar{\zeta})$ used to define I_o, Eq. (4.35)
EMOD	Modulus of elasticity
ET(2)	Table of moduli of elasticity
ETA	η, defined in Eq. (4.8)
FACT	Value of I_{o_n}/I_{o_1}
FACTI(90)	Tabulated values of fitting function I_{o_n}/I_{o_1}, plotted in Figure 4.7
FIM(3)	Impulse factor for 7075-T6A1 compared with 2024-T4A1
FPM(3)	Pressure asymptote factor for 7075-T6A1 compared with 2024-T4A1
FST	Snap-through factor
*IBPC	Structure code 1-beam 2-panel 3-cylinder

*IMAT	Material code 1-2024T4 Aluminum 2-7075T6 Aluminum
ISC(90)	Output array used to indicate level of damage
*ISL	Damage level code 1-light damage 2-moderate damage 3-heavy damage
*IVOPT	Vulnerability option code 1-given weapon yield, determine critical range 2-given duration of exponential forcing function, determine critical pressure level 3-given weapon yield and range, determine damage level 4-given curve of pressure vs time, determine damage level
KOK	Control constant set to 1 by RITER to indicate iteration concluded
NC	Control for calling SETUP only once
NCHI	Number of values in CHIT
NLDR	Number of values in CLDRT
*NPP	Number of points used to define pressure vs time curve
NTRIAL	Number of present trial in iterative process for options 1 and 2
NU	Number of values in UT
NZ	Number of values in ZETAT
NZETA	Number of values in ZTA2T
NZTAI	Number of values in ZETAI
NZTA1	Number of values in ZTA1T
OUT(2)	Output array for blast characteristics returned by HYPRA
PCR	Critical pressure for Youngdahl's method
PCRM	Critical pressure for Youngdahl's method, metric
PFACT	Value of P_{o_n}/P_{o_1}

PH(3)	Critical pressures for three damage levels
PHP	Critical pressure
PI	π
PO	Sea-level pressure
POI	Ratio of blast pressure to blast impulse
PP(20)	Value of pressure at time TPP
*PPM(20)	Value of pressure at time TPP, metric
PPR	Peak pressure of exponential forcing function
PPRM	Peak pressure of exponential forcing function, metric
PRFAC(102)	Tabulated values of fitting function P_{o_n}/P_{o_1}, plotted in Figure 4.6
*PY	Ratio of critical pressure to be used in modified Youngdahl procedure to the pressure asymptote for light damage
PZ(3)	Pressure asymptotes for three damage levels
PZERO	Pressure asymptote
R	Range
RHO	Material density
RHOO	Sea-level air density
RHOT(2)	Table of material densities
*RM	Range, metric
*ROT	Cylinder radius to thickness ratio
RTRIAL(3)	Trial ranges in iteration for option 1; inverse of trial pressure for option 2
SCHI	Value of $s(\chi)$ used in Eq. (4.28)
SF(5)	Scaling factors for blast calculations
SCHIT(31)	Tabulated values of fitting function $s(\chi)$ plotted in Figure 4.3
*SM	Longest distance from any point in face of structure containing beam or plate to farthest free edge

SMALT	Plate or beam thickness
SN2	Stress parameter, $\eta^2 s(\chi)$, in Eq. (4.28)
SN2A	Value of stress parameter, $\eta^2 s(\chi)$, just after snap-through
SN2B	Value of stress parameter, $\eta^2 s(\chi)$, just before snap-through
SRAE	Square root of product of density, area squared, and modulus of elasticity
*SSM	Distance from center of beam or plate to closest free edge
STFAC(39)	Tabulated values of snap-through factor plotted in Figure 4.9
*TO	Duration of exponential forcing function
*TM	Plate or beam thickness, metric
*TPP(20)	Time at which pressure is given
U	μ, defined in Eq. (4.9)
UT(13)	Values of μ used in tabulating data for snap-through factor plotted in Figure 4.9
W	Value of loading parameter, ω, defined in Eq. (4.16)
W1	Critical value of loading parameter, ω, defined in Eq. (4.16), for light damage
WL	Width over which pressure acts
*WM	Weapon yield, metric
WST	Value of loading parameter, ω, defined in Eq. (4.16), at snap-through
WW	Critical value of loading parameter, ω, defined in Eq. (4.16)
WY	Weapon yield
*XX	Input dummy: for beams, width over which loading acts, metric; for plates, aspect ratio
ZEROI	Impulse asymptote
ZETA	Value of tensile axial load parameter, ζ, defined in Eq. (4.19)

ZETAI(45) Values of $\bar{\zeta}$ used in tabulating data for I_{o_n}/I_{o_1} in Figure 4.7

ZETAT(31) Values of $\bar{\zeta}$ used in tabulating data for $\delta(\bar{\zeta})$ in Figure 4.4

ZI(3) Impulse asymptotes for three damage levels

ZTA1T(62) Values of $\bar{\zeta}$ used in tabulating data for $\beta(\bar{\zeta})$ in Figures 4.5 and 4.8

ZTA2T(51) Values of $\bar{\zeta}$ used in tabulating data for P_{o_n}/P_{o_1} in Figure 4.6

5.4 PIVUL Input

Card 1 (I12)

IVOPT, vulnerability option code

1-given weapon yield, determine critical range
2-given duration of exponential forcing function, determine critical pressure level
3-given weapon yield and range, determine damage level
4-given curve of pressure vs time, determine damage level

Note: Only options 1 and 3 can be used for cylinders.

Card 2 (Card 2 may be a single card or a group of cards, depending upon IVOPT)

IVOPT=1 (F12.1)

WM, weapon yield* (TJ)

IVOPT=2 (F12.1)

TO, duration of exponential forcing function (sec)

IVOPT=3 (2F12.1)

WM, weapon yield* (TJ)
RM, range (meters)

*The program does not include ground reflection effects, so the user must adjust the yield if appropriate to account for such effects.

IVOPT=4 (I12, (6F12.1))

NPP, number of points used to define pressure vs time curve ($\leq$20)

TPP(N), time at which pressure is given (sec)

PPM(N), value of pressure at time TPP(N) (kPa)

The first card contains NPP only.

Subsequent cards contains pairs of TPP(N) and PP(N), three pairs to a card. A total of NPP pairs must be provided. The first time must be 0.0. The last pressure must be 0.0.

Card 3 (F12.1)

PY, ratio of critical pressure to be used in modified Youngdahl procedure to P_{o_1}, the pressure asymptote for light damage. It is recommended that PY be assigned a value of 0.75.
If PY>1.0, the modified Youngdahl procedure is not used. PY must be positive. For cylinders, PY is not used, and any value may be put on the input card.

Card 4 (3I12)

IMAT, material code

1-2024T4 Aluminum
2-7075T6 Aluminum

IBPC, structure code

1-beam
2-panel
3-cylinder

ISL, damage level code (required only for IVOPT=1 or 2)

1-light damage
2-moderate damage
3-heavy damage

The following card(s) define the structure and some aspects of the loading. They depend upon the code IBPC, and will be given for each of the three possible values of IBPC.

IBPC=1

Card 5 (5F12.1)

BLM, beam length (meters)

CLDR, length to radius of curvature ratio ($0.0 \leq CLDR \leq 0.8$)

XX, width over which loading acts (meters)

SSM, distance from center of beam to closest free edge (meters) (omit for IVOPT=4)

SM, longest distance from any point in face of structure containing beam to farthest free edge (meters) (omit for IVOPT=4)

Card 6 (4F12.1)

ATOTM, cross-section area (sq cm)

CNTIM, cross-section area moment of inertia (cm^4)

CNTRM, distance from neutral axis to outer fiber on loaded side (cm)

TM, beam thickness (cm)

This completes the input for IBPC=1.

IBPC=2

Card 5 (5F12.1)

BLM, length of shorter side of panel (meters)

CLDR, ratio of BLM to radius of curvature in direction corresponding to BLM ($0.0 \leq CLDR \leq 0.8$)

AR, aspect ratio of plate, ratio of length of longer side to length of shorter side

SSM, distance from center of plate to closest free edge (meters) (omit for IVOPT=4)

SM, longest distance from any point in face of structure containing plate to farthest free edge (meters)(omit for IVOPT=4)

Card 6 (F12.1)

TM, plate thickness (cm)

This completes the input for IBPC=2.

IBPC=3

Card 5 (2F12.1)

ROT, radius to thickness ratio ($50 \leq ROT \leq 300$)

CLDD, length to diameter ratio ($1 \leq CLDD \leq 3$)

This completes the input for IBPC=3.

5.5 Program Operation and Output

The NOVA program is written in FORTRAN-IV and has been run on the Control Data Corporation 6600 scientific computer under the SCOPE (Supervisory Control of Program Execution) operating system, version 3.4.3. About 70,000 cells of central memory are required to compile PIVUL and 40,000 cells of central memory are required for program loading and execution. Computation time is on the order of 0.2 seconds.

Although the program output is largely self-explanatory, the normal output is described in detail in Table 5.1. The corresponding program variable is given parenthetically.

In addition, certain error situations can develop which will generate error messages, which are described in Table 5.2. In this connection, it should be noted that the user is responsible for observing the limits on input variables indicated in Subsection 5.4. Generally, erroneous input will not generate an error message. The input, or information directly devised from input, is printed out, however, so that the user should easily be able to identify that his problem is due to incorrect input.

TABLE 5.1

NORMAL OUTPUT

```
VULNERABILITY OPTION i (IVOPT)

For IVOPT=1,
     YIELD = X.XXXXXX  TJ (WM)
For IVOPT=2,
     DURATION = X.XXXXXX SEC (TO)
For IVOPT=3,
     YIELD = X.XXXXXX TJ AT RANGE OF X.XXXXXX METERS (WM, RM)
For IVOPT=4,
     TIME            PRESSURE
     (SEC)           (KPA)
     X.XXXXXX        X.XXXXXX
         ¦               ¦
         ¦               ¦
     X.XXXXXX        X.XXXXXX

YOUNGDAHLS METHOD, PCR/PO = X.XXXXXX (PY, output only if PY≤1.0)
     LIGHT DAMAGE or MODERATE DAMAGE or HEAVY DAMAGE
2024-T4 ALUMINUM or 7075-T6 ALUMINUM
BEAM or PANEL or CYLINDER

For beams (IBPC=1),
     LENGTH = X.XXXXXX METERS  (BLM)
     L/R = X.XXXXXX  (CLDR)
     LOADING WIDTH = X.XXXXXX METERS (XX)
   * SHORTEST DISTANCE TO FREE EDGE = X.XXXXXX METERS (SSM)
   * LONGEST DISTANCE FROM ANY POINT TO FREE EDGE = X.XXXXXX METERS (SM)
CROSS-SECTION DATA
     AREA = X.XXXXXX SQ CM (ATOTM)
     MOMENT OF INERTIA = X.XXXXXX CM**4 (CNTIM)
     DISTANCE TO OUTSIDE FIBER ON LOADED SIDE = X.XXXXXX CM (CNTRM)
     THICKNESS = X.XXXXXX CM(TM)
```

*Omitted for IVOPT=4.

TABLE 5.1 (Concluded)

For panels (IBPC=2)

LENGTH = X.XXXXXX METERS (BLM)

L/R = X.XXXXXX (CLDR)

ASPECT RATIO = X.XXXXXX (AR)

*SHORTEST DISTANCE TO FREE EDGE = X.XXXXXX METERS (SSM)

*LONGEST DISTANCE FROM ANY POINT TO FREE EDGE = X.XXXXXX METERS (SM)

THICKNESS = X.XXXXXX CM (TM)

For cylinders (IBPC=3)

R/T = X.XXXXXX (ROT)

L/D = X.XXXXXX (CLDD)

PCR FOR YOUNGDAHLS METHOD = X.XXXXXX KPA (PCRM, output only if PY≤1.0)

For IVOPT=1,

CRITICAL RANGE = X.XXXXXX METERS (RM)

FOR IVOPT=2,

CRITICAL FREE-FIELD OVERPRESSURE = X.XXXXXX KPA (PPRM)

For IVOPT=3 or 4,

ZERO RESPONSE	LIGHT DAMAGE	MODERATE DAMAGE	HEAVY DAMAGE
Y	Y	Y	Y

X

*Omitted for IVOPT=4.

TABLE 5.2

ERROR MESSAGES

CHI = X.XXXXXX CHECK BEAM CROSS-SECTION DATA

This message is printed out by BEAM if CHI>1 is not possible, the beam cross-section data must be in error. Program stops.

C VS R CURVE SLOPE REVERSAL

This message is printed out by RITER if the response criterion, CRIT, has decreased with decreasing range (or increasing pressure). This violates the assumption of RITER that the criterion increases monotonically with increasing pressure. Program stops.

ERROR STOP - CRITICAL PRESSURE FOR YOUNGDAHL IS GREATER THAN PEAK APPLIED PRESSURE

For option 3 or 4, the peak pressure in the forcing function is smaller than PCR, thus making Youngdahl integrations invalid. IVULT prints out this message and program stops.

ERROR STOP - DAMAGE LEVEL iiiiii NOT ALLOWED

The damage level code is less than 1 or greater than 3. PIVUL prints out this message and program stops.

ERROR STOP - DIFFRACTION LOADING PERIOD TOO LONG - CHECK SM AND SSM

This message is printed out by SIDE if the diffractive clearing time is greater than the forcing function duration. User should check values of input variables SM and SSM. Program stops.

FIRST ARGUMENT IS OUTSIDE TABLE, X=X.XXXXXX
XT = X.XXXXXX.....X.XXXXXX

This message is printed out by INTERP if the first independent variable, X, falls outside the range of tabulated data. The value of the first independent variable and the corresponding table values are printed out. Program stops.

RANGE ITERATION IS NOT CONVERGING

To avoid a possible iteration loop in searching for the critical range or pressure, the number of trials allowed is restricted to twelve. This message is printed out by RITER to indicate that adequate convergence has not been achieved in twelve trials. Program stops.

SECOND ARGUMENT IS OUTSIDE TABLE, Y=X.XXXXXX
YT = X.XXXXXX.....X.XXXXXX

This message is printed out by INTERP if the second independent variable, Y, falls outside the range of tabulated data. The value of the second independent variable and the corresponding table values are printed out. Program stops.

TABLE 5.2 (Concluded)

THIRD ARGUMENT IS OUTSIDE TABLE, Z = X.XXXXXX
ZT = X.XXXXXX.....X.XXXXXX
This message is printed out by INTERP if the third independent variable, Z, falls outside the range of tabulated data. The value of the third independent variable and the corresponding table values are printed out. Program stops.

VULNERABILITY OPTION i NOT ALLOWED FOR CYLINDERS
Vulnerability option 2 or 4 has been specified for a cylinder. PIVUL prints out this message and program stops.

X-VALUE X.XXXXX OUTSIDE TABLE. Y-VALUE RETURNED
= X.XXXXXX X-TABLE = X.XXXXXX.....X.XXXXXX
This message is pointed out by INT1 if the independent variable, X, falls outside the range of tabulated data. The value of the independent variable and the table values are printed out. The dependent variable, Y, will be the minimum or maximum table value, depending upon whether X falls below or above the tabulated data. Program stops.

5.6 Example Problem

The structure for the example problem is a curved panel. The required dimensions and material are:

Thickness = 0.08 cm

Length of short side = 0.2 meters

Length to radius of curvature ratio = 0.05

Aspect ratio = 1.3

Material = 2024T4 Al

Distance from center of plate to closest free edge = 1 meter

Longest distance from any point in face of structure containing plate to farthest free edge = 3 meters

It is desired to determine the level of response of this structure at a range of 300 meters from a 4.2 TJ explosion (the value 4.2 is an effective yield which includes enhancement by ground effects). The modified Youngdahl approach is to be used, with a ratio of critical pressure to P_{o_1} of 0.75.

The input data deck is as follows:

```
3
4.2     300.
0.75
1       2
0.2     0.05     1.3     1.0     3.0
0.08
```

The resulting output is reproduced below.

```
VULNERABILITY OPTION 5

YIELD =    .420000E+01 TO AT RANGE OF    .300000E+05 METERS

YOUNGDAHLS METHOD, PCR/PO =    .750000E+00

2024-T4 ALUMINUM
PANEL
LENGTH =    .200000E+00 METERS          L/H =    .500000E-01
ASPECT RATIO =    .150000E+01
SHORTEST DISTANCE TO FREE EDGE =    .100000E+01 METERS
LONGEST DISTANCE FROM ANY POINT TO FREE EDGE =    .300000E+01 METERS
THICKNESS =    .800000E-01 CM

PCR FOR YOUNGDAHLS METHOD =    .235456E+02 KPA

      ZERO              LIGHT             MODERATE              HEAVY
    RESPONSE           DAMAGE             DAMAGE              DAMAGE
       Y                 Y                  Y                   Y
                                              X
```

The output shows that the structure experiences an amount of damage between moderate and heavy for the specified conditions.

SECTION 6
CONCLUSIONS AND RECOMMENDATIONS

This report has presented the methodology which led to the development of a vulnerability code for utilization in rapid damage assessment of simple structural elements subjected to a nuclear blast environment. In the development of the methodology, structural models typifying a variety of representative straight and curved beam, flat and curved plate, and cylinder configurations were analytically loaded with simulated nuclear blast overpressure time-histories and light, moderate, and heavy damage levels of response were defined by using pressure-impulse analyses. The structural model support constraints considered were fixed-fixed end conditions for the beams, plates, and cylinders; the materials of construction considered were both 2024-T4 and 7075-T6 aluminum alloys. During the course of the investigation, several general conclusions and recommendations were arrived at and are presented in the paragraphs which follow.

The moment gradient which exists at the ends of a thin fixed-fixed beam is extremely steep, due to the assumed boundary condition of a perfectly rigid support. This steep moment gradient in turn results in localized, extremely severe strains at the ends of the beam. Response criteria based on these highly localized strains may be too severe in terms of the improbability of attaining a perfectly rigid support in real construction. Edge fastenings, which are not modeled, may be of importance.

The use of static elastic analysis solutions as a guide in selecting appropriate fitting functions for the P-I data generated proved to be very helpful. The particular success achieved in applying the method to the large amount of 2024 straight beam data generated resulted in a fairly high degree of confidence in the resulting 2024 straight beam fitting functions. Somewhat less confidence is assigned to the 2024 curved beam fitting functions due to the added complexity posed by the curved beam snap-through problem.

Since a lesser amount of P-I data were generated for 7075 structures than for 2024 structures, it was necessary to employ conversion factors to relate the selected 7075 fitting functions to the previously selected 2024 fitting functions. Consequently, the 7075 fitting functions are considered to be not quite as good as the 2024 fitting functions. However, if more 7075 P-I data were available, static elastic analysis could again be utilized as a guide in selecting 7075 fitting functions which would result in a higher degree of confidence.

The vulnerability assessment code which has been developed herein is satisfactory for providing rapid, approximate answers as to the relative hardness of simple structural elements subjected to nuclear blast overpressure loadings. Furthermore, the code should prove to be a valuable tool when used either in the preliminary designs of future military weapon systems or in the analysis of presently existing systems.

Typical of any analytical tool development, the vulnerability code presented herein requires experimental verification. It is recommended that experimental verification begin with the 2024 straight beam. If such experimental verification is successful, experiments should be run for correlation with the 2024 curved beam and 2024 plate analyses.

If the experimental verification is successful, further analytical efforts should be undertaken to obtain more accurate fitting functions for the 7075 aluminum elements and to develop data for other materials.

REFERENCES

1. Sperrazza, J., Dependence of External Blast Damage to the A-25 Aircraft on Peak Pressure and Impulse, Memorandum Report 575, USA Ballistic Research Laboratories, APG, Maryland, September 1951. (AD#378275)

2. Youngdahl, C.K., "Correlation Parameters for Eliminating the Effect of Pulse Shape on Dynamic Plastic Deformation", Journal of Applied Mechanics, Transactions of the ASME, pp. 744-752, September 1970.

3. Schumacher, R., and Cummings, B., A Modified Pressure-Impulse Blast Damage Model, BRL MR 2724, AD No. A036196, USA Ballistic Research Laboratory, APG, Maryland, January 1977.

4. ALCOA Structural Handbook, Aluminum Company of America, Pittsburgh, Pa., 1958.

5. NOVA - A Digital Computer Program for Calculating the Response of Aircraft to the Overpressure from a Nuclear Weapon, Vol. I - Theory and Program Description, Prepared by Kaman AviDyne for the AFWL, AFWL-TR-72-115, Vol. I, July 1973.

6. Dunn, B.J., Lavagnino, A., and White, J.J., Parametric Analysis of Nuclear Weapon Air Blast Effects on a Model Target, BDM/W-74-009TR, Braddock, Dunn and McDonald, Inc., December 1973.

7. Mente, L.J., The Dynamic, Elastic-Plastic, Large Displacement Response of Buckling Sensitive Cylindrical Shells to Blast-Type Loadings, -- Part I Analytical Formulation, AMC-2-68-(T), Kaman AviDyne TR-53, Kaman Sciences Corporation, August 1968.

8. NOVA-2 - A Digital Computer Program for Analyzing Nuclear Overpressure Effects on Aircraft, Prepared by Kaman AviDyne for the AFWL, KA TR-128, (to be published).

APPENDIX A

VARIATION IN P-I CURVE WITH FORCING FUNCTION

A pressure-impulse curve is constructed for a given forcing function time-history, and a P-I curve should be used cautiously for other forcing functions. This appendix addresses the question of how much the P-I curve varies with forcing function for a simple class of forcing functions typical of blast-type loadings.

The forcing function used for this purpose is shown in Figure A.1, and consists simply of the superposition of two triangular forcing functions of different durations. The amplitude of the longer duration triangle is one-half the amplitude of the total forcing function at time zero. The parameter which is used to obtain different forcing functions is the duration ratio, t_1/t_o.

The structure for which the forcing functions were applied was a 2024-T4 aluminum I-beam, with a length to height ratio of 35 and area ratios $A_2/A_1 = 0.9$ and $A_3/A_1 = 1.0$. The light damage case was examined.

The resulting P-I curves are given in Figure A.2 for duration ratios of 0.01, 0.5, and 1.0. The pressure and impulse are normalized to the pressure and impulse asymptotes, respectively. The range of duration ratios covers the extremes: The value of 0.01 corresponds to a very sharp spike at the beginning, while the value of 1.0 results in just a simple triangular forcing function.

The variation between the two extreme curves is seen to be significant. To quantify the significance, suppose an analyst has a pressure-time curve of given duration and wants to know the magnitude of the pressure required to produce damage. A given duration defines a straight line through the origin of the P-I plane. Hence, the ratio of the pressure from the two extreme curves along a line through the origin is the desired measure of the significance of the variation in the P-I curves. The largest value of this ratio occurs along the line defined by the normalized pressure and the normalized impulse being equal (a 45° line if the horizontal and vertical scales are the same, as in Figure A.2), and is approximately 1.4. Hence, if the analyst had a P-I curve based on a duration ratio of 0.01 available and was interested in a simple triangular forcing function (duration ratio = 1), he would overpredict the pressure required by 40% at most. If he had a P-I curve midway between the extreme curves on Figure A.3 he could not be in error by more than 20%.

It should be remembered that the above errors result when considering only forcing functions of the class depicted by Figure A.1. For other forcing functions, such as a ramp or a half sine, the error could be significantly greater.

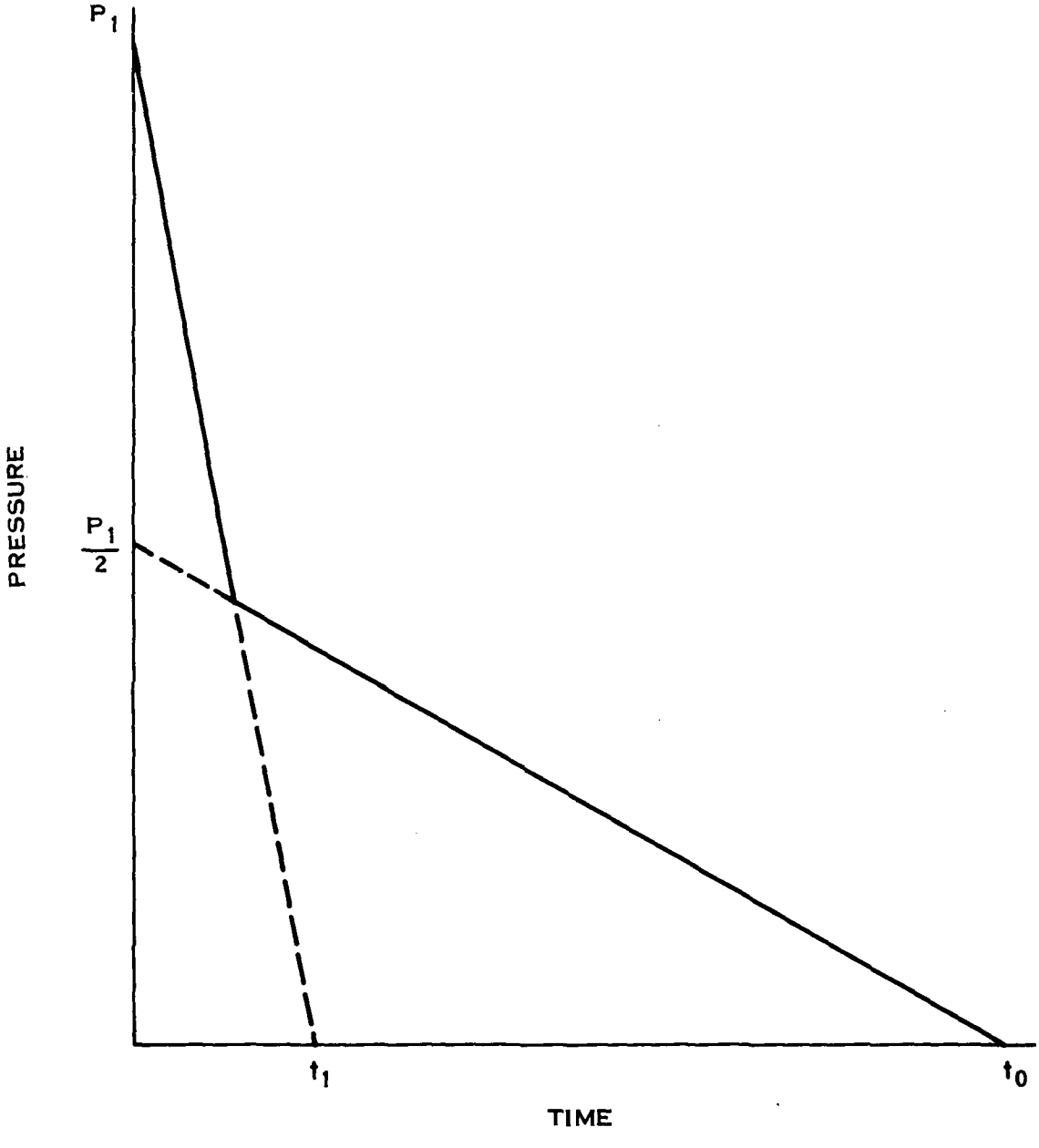

FIGURE A.1 PRESSURE VS TIME

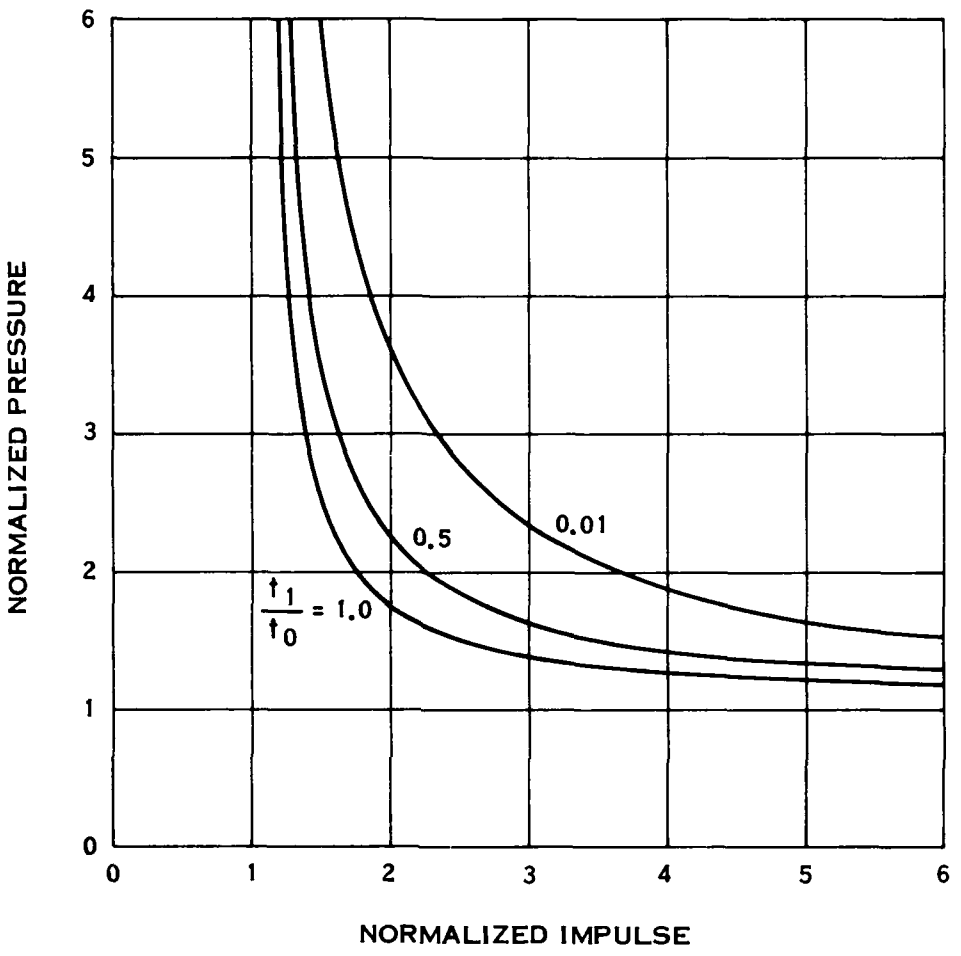

FIGURE A.2 VARIATION OF P–I CURVE WITH FORCING FUNCTION

DISTRIBUTION LIST

No. of Copies	Organization
12	Commander Defense Technical Info Center ATTN: DDC-DDA Cameron Station Alexandria, VA 22314
4	Director of Defense Research and Engineering ATTN: DD/TWP DD/S&SS DD/I&SS AD/SW Washington, DC 20301
2	Asst. to the Secretary of Defense (Atomic Energy) ATTN: Document Control Donald R. Cotter Washington, DC 20301
3	Director Defense Advanced Research Projects Agency ATTN: Tech Lib NMRO PMO 1400 Wilson Boulevard Arlington, VA 22209
2	Director Defense Civil Preparedness Agency ATTN: Mr. George Sisson/RF-SR Technical Library Washington, DC 20301
4	Director Defense Intelligence Agency ATTN: DT-1B DB-4C/E. O. Farrell DT-2/Wpns & Sys Div RDS-344 Washington, DC 20301
1	Director Weapons Systems Evaluation Gp ATTN: Document Control Washington, DC 20305
1	Director National Security Agency ATTN: E. F. Butala, R15 Ft. George G. Meade, MD 20755
3	Director Joint Strategic Target Planning Staff JCS ATTN: Sci & Tech Info Lib JLTW-2 DOXT Offut AFB Omaha, NM 68113
1	Director Defense Communications Agency ATTN: Code 930 Washington, DC 20305
5	Director Defense Nuclear Agency ATTN: STSI/Archives SPAS/Mr. J. Moulton STSP STVL/Dr. La Vier RATN Washington, DC 20305
6	Director Defense Nuclear Agency ATTN: DDST/Dr. Conrad DDST/Dr. Oswald STTL/Tech Lib (2 cys) SPSS (2 cys) Washington, DC 20305

DISTRIBUTION LIST

No. of Copies	Organization
2	Commander Field Command, DNA ATTN: FCPR FCTMOF Kirtland AFB, NM 87115
1	Commander Field Command, DNA Livermore Branch ATTN: FCPRL P.O. Box 808 Livermore, CA 94550
1	Director Institute for Defense Analyses ATTN: IDA Librarian Ruth S. Smith 400 Army-Navy Drive Arlington, VA 22202
2	HQDA (DAMA-AR; NCL Div) Washington, DC 20310
1	Program Manager US Army BMD Program Office ATTN: John Shea 5001 Eisenhower Avenue Alexandria, VA 22333
2	Director US Army BMD Advanced Technology Center ATTN: CRDABH-X CRDABH-S Huntsville, AL 35807
1	Commander US Army BMD System Command ATTN: BDMSC-TFN/N.J. Hurst P.O. Box 1500 Huntsville, AL 35807
2	Deputy Chief of Staff for Operations and Plans ATTN: Technical Library Director of Chemical and Nuclear Operations Department of the Army Washington, DC 20310
2	Office, Chief of Engineers Department of the Army ATTN: DAEN-MCE-D DAEN-RDM 890 South Pickett Street Alexandria, VA 22304
1	Commander US Army Engineering Center ATTN: ATSEN-SY-L Fort Belvoir, VA 22060
1	Division Engineer US Army Engineering Division ATTN: HNDSE-R/M.M. Dembo Huntsville Box 1600 Huntsville, AL 35804
1	Division Engineer US Army Engineering Division Ohio River ATTN: Docu Cen P.O. Box 1159 Cincinnati, OH 45201
5	Commander US Army Engineer Waterways Experiment Station ATTN: Technical Library William Flathau John N. Strange Guy Jackson Leo Ingram P.O. Box 631 Vicksburg, MS 39180

DISTRIBUTION LIST

No. of Copies	Organization
1	Commander US Army Materiel Development and Readiness Command ATTN: DRCDMD-ST 5001 Eisenhower Avenue Alexandria, VA 22333
1	Commander US Army Materiel Development & Readiness Command ATTN: Technical Library 5001 Eisenhower Avenue Alexandria, VA 22333
3	Commander US Army Armament Research & Development Command ATTN: DRDAR-LCN-F, W. Reiner DRDAR-TSS (2 cys) Dover, NJ 07801
1	Director US Army ARRADCOM Benet Weapons Laboratory ATTN: DRDAR-LCB-TL Watervliet, NY 12189
1	Commander US Army Armament Materiel Readiness Command ATTN: DRSAR-LEP-L, Tech Lib Rock Island, IL 61299
1	Commander US Army Aviation Research & Development Command ATTN: DRSAV-E P.O. Box 209 St. Louis, MO 63166
1	Director US Army Air Mobility Research & Development Laboratory Ames Research Center Moffett Field, CA 94035
1	Commander US Army Communications Research & Development Command ATTN: DRDCO-PPA-SA Fort Monmouth, NJ 07703
6	Commander US Army Electronics Research & Development Command ATTN: DELSD-L DELEW-E W. S. McAfee R. Freiberg DELSD-EI, J. Roma DELSD-EM A. Sigismondi C. Goldy Fort Monmouth, NJ 07703
5	Commander US Army Harry Diamond Labs ATTN: Mr. James Gaul Mr. L. Belliveau Mr. J. Gwaltney Mr. F.N. Wimenitz Mr. Bill Vault 2800 Powder Mill Road Adelphi, MD 20783
5	Commander US Army Harry Diamond Labs ATTN: DRXDO-TI DRXDO-TI/012 DRXDO-NP DRXDO-RBH/P. Caldwell DELHD-RBA/J. Rosado 2800 Powder Mill Road Adelphi, MD 20783
3	Commander US Army Missile Command ATTN: DRDMI-R DRDMI-YDL Chief Scientist Redstone Arsenal, AL 35809

DISTRIBUTION LIST

No. of Copies	Organization
2	Commander US Army Natick Research & Development Command ATTN: DRXRE/Dr.D. Sieling DRXNM-UE Arthur Johnson Natick, MA 01762
1	Commander US Army Tank Automotive Rsch & Development Command ATTN: DRDTA-UL Warren, MI 48090
1	Commander US Army Foreign Science and Technology Center ATTN: Rsch & Concepts Branch 220 7th Street, NE Charlottesville, VA 22901
1	Commander US Army Logistical Center ATTN: ATCL-SCA Mr. Robert Cameron Fort Lee, VA 23801
3	Commander US Army Materials and Mechanics Research Center ATTN: Technical Library John Mescall Richard Shea Watertown, MA 02172
2	Commander US Army Nuclear Agency ATTN: ACTA-NAW Technical Library 7500 Backlick Road, Bldg.2073 Springfield, VA 22150
1	Commander US Army Research Office P.O. Box 12211 Research Triangle Park NC 27709
1	Commander US Army Training & Doctrine Cmd ATTN: ATCD-SA/Mr. Oscar Wells Fort Monroe, VA 23651
2	Director US Army TRADOC Systems Analysis Activity ATTN: LTC John Hesse ATAA-SL (Tech Lib) White Sands Missile Range NM 88002
1	Commander Combined Arms Combat Developments Activity ATTN: ATCA-CO/Mr.L.C. Pleger Fort Leavenworth, KS 66027
1	Chief of Naval Research ATTN: N. Perrone Department of the Navy Washington, DC 20360
2	Chief of Naval Operations ATTN: OP-03EG OP-985F Department of the Navy Washington, DC 20350
1	Chief of Naval Material ATTN: MAT 0323 Department of the Navy Arlington, VA 22217

DISTRIBUTION LIST

No. of Copies	Organization
3	Director Strategic Systems Projects Ofc ATTN: NSP-43, Tech Lib NSP-273 NSP-272 Department of the Navy Washington, DC 20360
1	Commander Naval Electronic Systems Cmd ATTN: PME 117-21A Washington, DC 20360
3	Commander Naval Facilities Engineering Command ATTN: Code 03A Code 04B Technical Library Washington, DC 20360
2	Commander Naval Sea Systems Command ATTN: ORD-91313 Library Code 03511 Department of the Navy Washington, DC 20362
4	Officer-in-Charge Civil Engineering Laboratory Naval Constr Btn Ctr ATTN: Stan Takahashi R.J. Odello John Crawford Technical Library Port Hueneme, CA 93041
2	Commander Naval Ship Engineering Center ATTN: Technical Library NSEC 6105G Hyattsville, MD 20782
1	Commander David W. Taylor Naval Ship Research & Development Center ATTN: Lib Div, Code 522 Bethseda, MD 22084
1	Commander Naval Surface Weapons Center ATTN: DX-21, Library Br. Dahlgren, VA 22448
3	Commander Naval Surface Weapons Center ATTN: Code WA501/Navy Nuclear Programs Office Code WX21/Tech Lib Code 240/C.J. Aronson Silver Spring, MD 20910
2	Commander Naval Weapons Center ATTN: Code 533/Tech Lib Code 40701/M.Keith China Lake, CA 94555
2	Commander Naval Ship Research & Development Center Facility Underwater Explosions Rsch Div ATTN: Code 17/W.W. Murray Technical Library Portsmouth, VA 23709
2	Commander Naval Weapons Evaluation Facility ATTN: Document Control R. Hughes Kirtland AFB Albuquerque, NM 87117
2	Director Naval Research Laboratory ATTN: Code 2027/Tech Lib Code 8440/F. Rosenthal Washington, DC 20375

AD-A085 715 KAMAN AVIDYNE BURLINGTON MA F/G 18/3
PIVUL - A COMPUTER CODE FOR RAPID ASSESSMENT OF THE VULNERABILI--ETC(U)
MAR 80 N P HOBBS, K R WETMORE DAAD05-76-C-0742
UNCLASSIFIED KA-TR-125 ARBRL-CR-00417 NL

2 OF 2

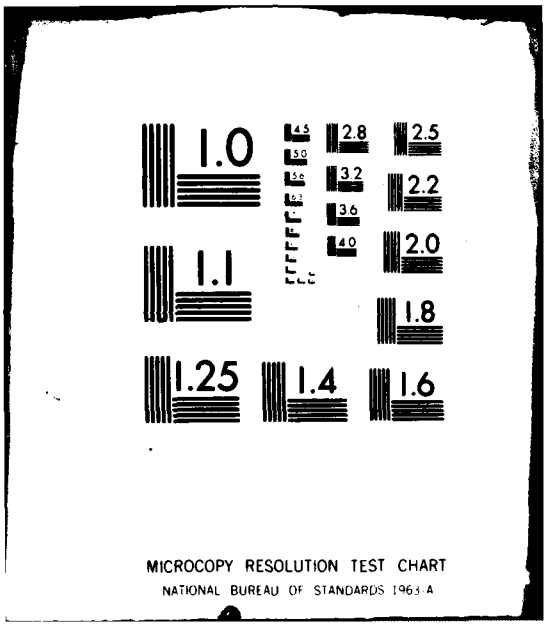
1.0
1.1
1.25
1.4
1.6
1.8
2.0
2.2
2.5
2.8
3.2
3.6
4.0
4.5
5.0
5.6
6.3
7.1
8.0
9.0
10.0
MICROCOPY RESOLUTION TEST CHART
NATIONAL BUREAU OF STANDARDS 1963-A

DISTRIBUTION LIST

No. of Copies	Organization
1	Superintendent Naval Postgraduate School ATTN: Code 2124/Tech Rpts Lib Monterey, CA 93940
1	HQ USAF (IN) Washington, DC 20330
1	HQ USAF (PRE) Washington, DC 20330
2	AFSC (DLCAW; Tech Lib) Andrews AFB Washington, DC 20331
2	AFATL (DLYV, P. Nash) Eglin AFB, FL 32542
1	AFATL (DLYV, Jim Flint) Eglin AFB, FL 32542
2	ADTC (ADBRL-2; Tech Lib) Eglin AFB, FL 32542
2	RADC (EMTLD/Docu Lib; EMREC/ R.W. Mair) Griffis AFB, NY 13340
1	AFWL/DE-I Kirtland AFB, NM 87117
1	AFWL/DEX Kirtland AFB, NM 87117
1	AFWL/SUL Jimmie L. Bratton Kirtland AFB, NM 87117
1	AFWL/R.Henny Kirtland AFB, NM 87117
1	AFWL/SUL M.A. Plamondon Kirtland AFB, NM 87117
1	Interservice Nuclear Weapons School ATTN: Technical Library Kirtland AFB, NM 87115
2	Commander-in-Chief Strategic Air Command ATTN: NRI-STINFO Lib XPFS Offutt AFB, NB 68113
4	FTD (TDFBD; TDPMG; ETET/ CPT R.C. Husemann; TD-BTA/Lib) Wright-Patterson AFB, OH 45433
1	AFIT (Lib Bldg. 640, Area B) Wright-Patterson AFB OH 45433
1	Director US Bureau of Mines ATTN: Technical Library Denver Federal Center Denver, CO 80225
1	Director US Bureau of Mines Twin Cities Research Center ATTN: Technical Library P.O. Box 1660 Minneapolis, MN 55111
1	US Energy Res & Dev Admin Albuquerque Operations Office ATTN: Doc Control for Tech Lib P.O. Box 5400 Albuquerque, NM 87115
1	US Energy Research and Development Administration Nevada Operations Office ATTN: Doc Control for Tech Lib P.O. Box 14100 Las Vegas, NV 89114

DISTRIBUTION LIST

No. of Copies	Organization
1	Director Lawrence Livermore Lab ATTN: L.W. Woodruft/L-96 P.O. Box 808 Livermore, CA 94550
1	Director Lawrence Livermore Lab ATTN: Jack Kahn/L-7 P.O. Box 808 Livermore, CA 94550
1	Director Lawrence Livermore Lab ATTN: Tech Info Dept L-3 P.O. Box 808 Livermore, CA 94550
1	Director Lawrence Livermore Lab ATTN: R.G. Dong/L-90 P.O. Box 808 Livermore, CA 94550
1	Director Lawrence Livermore Lab ATTN: Ted Butkovich/L-200 P.O. Box 808 Livermore, CA 94550
1	Director Lawrence Livermore Lab ATTN: Robert Schock/L-437 P.O. Box 808 Livermore, CA 94550
1	Director Lawrence Livermore Lab ATTN: J.R. Hearst/L-205 P.O. Box 808 Livermore, CA 94550
4	Director Los Alamos Scientific Lab ATTN: Doc Control for Rpts Lib R.A. Gentry G.R. Spillman Al Davis P.O. Box 1663 Los Alamos, NM 87544
6	Sandia Laboratories ATTN: Doc Control for 3141 Sandia Rpt Collection A.M. Chaban M.L. Merritt L.J. Vortman W. Roherty L. Hill P.O. Box 5800 Albuquerque, NM 87115
1	Sandia Laboratories Livermore Laboratory ATTN: Doc Control for Tech Lib P.O. Box 969 Livermore, CA 94550
1	Director National Aeronautics and Space Administration Scientific and Technical Information Facility P.O. Box 8757 Baltimore/Washington International Airport, MD 21240
3	Aerospace Corporation ATTN: Tech Info Services(2 cys) P.N. Mathur P.O. Box 92957 Los Angeles, CA 90009
1	Agabian Associates ATTN: M. Agbabian 250 North Nash Street El Segundo, CA 90245

DISTRIBUTION LIST

No. of Copies	Organization
1	Applied Theory, Inc. ATTN: John G. Trulio 1010 Westwood Blvd. Los Angeles, CA 90024
1	Artec Associates, Inc. ATTN: Steven Gill 26046 Eden Landing Road Hayward, CA 94545
1	AVCO ATTN: Res Lib A830, Rm 7201 201 Lowell Street Wilmington, MA 01887
1	The BDM Corporation ATTN: Richard Hensley P.O. Box 9274 Albuquerque International Albuquerque, NM 87119
2	The Boeing Company ATTN: Aerospace Library R.H. Carlson P.O. Box 3707 Seattle, WA 98124
1	Brown Engineering Co., Inc. ATTN: Manu Patel Cummings Research Park Huntsville, AL 35807
2	California Research and Technology, Inc. ATTN: Ken Kreyenhagen Technical Library 6269 Variel Avenue Woodland Hills, CA 91364
1	Calspan Corporation ATTN: Technical Library P.O. Box 235 Buffalo, NY 14221
1	Civil/Nuclear Systems Corp. ATTN: Robert Crawford 1200 University N.E. Albuquerque, NM 87102
1	EG&G Incorporated Albuquerque Division ATTN: Technical Library P.O. Box 10218 Albuquerque, NM 87114
1	The Franklin Institute ATTN: Zemons Zudans 20th Street and Parkway Philadelphia, PA 19103
1	General American Trans Corp. General American Research Div. ATTN: G.L. Neidhardt 7449 N. Natchez Avenue Niles, IL 60648
1	General Electric Company-TEMPO ATTN: DASIAC P.O. Drawer QQ Santa Barbara, CA 93102
1	General Electric-TEMPO ATTN: E. Bryant 220 S. Main Street, Rm 206 Bel Air, MD 21014
2	Hazeltine Corp. ATTN: Carl Meinen Greenlawn, NY 11740
1	J.H. Wiggins Co., Inc. ATTN: John Collins 1650 South Pacific Coast Hghwy Redondo Beach, CA 90277

DISTRIBUTION LIST

No. of Copies	Organization
6	Kaman Avidyne ATTN: Dr. N.P. Hobbs (4 cys) Kenneth R. Wetmore MR. S. Criscione 83 Second Avenue Northwest Industrial Park Burlington, MA 01830
3	Kaman Sciences Corporation ATTN: Library P.A. Ellis F.H. Shelton 1500 Garden of the Gods Road Colorado Springs, CO 80907
1	Lockheed Missiles & Space Co. ATTN: Technical Library P.O. Box 504 Sunnyvale, CA 94088
2	Martin Marietta Aerospace *Orlando Division* ATTN: G. Fotieo Mail Point 505, Craig Luongo P.O. Box 5837 Orlando, FL 32805
3	McDonnell Douglas Astronautics Corporation ATTN: Robert W. Halprin Mr. C. Gardiner Dr. P. Lewis 5301 Bolsa Avenue Huntington Beach, CA 92647
2	Merritt Cases, Inc. ATTN: J.L. Merritt Techical Library P.O. Box 1206 Redlands, CA 92373
1	Meteorology Research, Inc. ATTN: W.D. Green 454 West Woodbury Road Altadena, CA 91001
1	The Mitre Corporation ATTN: Library P.O. Box 208 Bedford, MA 01730
1	Pacific Sierra Research Corp. ATTN: Dr. Harold Brode 1456 Cloverfield Boulevard Santa Monica, CA 90404
2	Pacifica Technology ATTN: G. Kent R. Bjork P.O. Box 148 Del Mar, CA 92014
4	Physics International Corp. ATTN: Robert Swift Charles Godfrey Larry A. Behrmann Technical Library 2700 Merced Street San Leandro, CA 94577
1	Radkowski Associates ATTN: Peter R. Radkowski P.O. Box 5474 Riverside, CA 92517
2	R&D Associates ATTN: Dr. Albert L. Latter William B. Wright P.O. Box 9695 Marina del Rey, CA 90291
4	R&D Associates ATTN: Jerry Carpenter Sheldon Schuster J.G. Lewis Technical Library P.O. Box 9695 Marina del Rey, CA 90291

DISTRIBUTION LIST

No. of Copies	Organization
1	R&D Associates ATTN: Henry Cooper Suite 500 1401 Wilson Boulevard Arlington, VA 22209
1	The Rand Corporation ATTN: C.C. Mow 1700 Main Street Santa Monica, CA 90406
2	Science Applications, Inc. ATTN: William Layson John Cockayne 8400 Westpark Drive McLean, VA 22102
1	Science Applications, Inc. 2450 Washington Avenue Suite 120 San Leandro, CA 94577
2	Science Applications, Inc. ATTN: Technical Library Michael McKay P.O. Box 2351 La Jolla, CA 92038
4	Systems, Science & Software ATTN: Donald R. Grine Ted Cherry Thomas D. Riney Technical Library P.O. Box 1620 La Jolla, CA 92037
3	Terra Tek, Inc. ATTN: Sidney Green A.H. Jones Technical Library 420 Wakara Way Salt Lake City, UT 84108
2	Tetra Tech, Inc. ATTN: Li-San Hwang Technical Library 630 North Rosemead Blvd. Pasadena, CA 91107
7	TRW Systems Group ATTN: Paul Lieberman Benjamin Sussholtz Norm Lipner William Rowan Jack Farrell Pravin Bhutta Tech Info Ctr/S-1930 One Space Park Redondo Beach, CA 92078
1	TRW Systems Group San Bernardino Operations ATTN: Greg Hulcher P.O. Box 1310 San Bernardina, CA 92402
2	Union Carbide Corporation Holifield National Laboratory ATTN: Doc Control for Tech Lib Civil Defense Research Proj P.O. Box X Oak Ridge, TN 37830
1	Universal Analytics, Inc. ATTN: E.I. Field 7740 W. Manchester Blvd. Playa del Rey, CA 90291
1	Weidlinger Assoc. Consulting Engineers ATTN: M.L. Baron 110 East 59th Street New York, NY 10022
1	Westinghouse Electric Co. Marine Division ATTN: W.A. Votz Hendy Avenue Sunnyvale, CA 94008

DISTRIBUTION LIST

No. of Copies	Organization
2	Battelle Memorial Institute ATTN: Technical Library R.W. Klingesmith 505 King Avenue Columbus, OH 43201
1	California Institute of Technology ATTN: T.J. Ahrens 1201 E. California Blvd. Pasadena, CA 91109
2	Denver Research Institute University of Denver ATTN: Mr. J. Wisotski Technical Library P.O. Box 10127 Denver, CO 80210
3	IIT Research Institute ATTN: Milton R. Johnson R.E. Welch Technical Library 10 West 35th Street Chicago, IL 60616
2	Lovelace Foundation for Medical Education ATTN: Asst. Dir of Research/ Robert K. Jones Technical Library 5200 Gibson Blvd., SE Albuquerque, NM 87109
1	Massachusetts Institute of Technology Aeroelastic and Structures Research Laboratory ATTN: Dr. E.A. Witmer Cambridge, MA 02139
2	Southwest Research Institute ATTN: Dr. W.E. Baker A.B. Wenzel 8500 Culebra Road San Antonio, TX 78206
2	SRI International ATTN: Dr. G.R. Abrahamson Carl Peterson 333 Ravenswood Avenue Menlo Park, CA 94025
1	University of Dayton Industrial Security Super. KL-505 ATTN: H.F. Swift 300 College Park Avenue Dayton, OH 45409
1	University of Illinois Consulting Engineering Services ATTN: Nathan M. Newmark 1211 Civil Engineering Bldg Urbana, IL 61801
2	The University of New Mexico The Eric H. Wang Civil Engineering Research Facility ATTN: Larry Bickle Neal Baum University Station Box 188 Albuquerque, NM 87131
2	Washington State University Administration Office ATTN: Arthur Miles Hohorf George Duval Pullman, WA 99163
	Aberdeen Proving Ground
	Dir, USAMSAA ATTN: DRXSY-D DRXSY-MP, H. Cohen Ben Cummings M.Reches
	Cdr,USATECOM ATTN: DRSTE-TO-F
	Dir, Wpns Sys Concepts Team Bldg E3516,EA ATTN: DRDAR-ACW
	Cdr,USAOC&S ATTN: ATSL-CD-CS/LT C.E. Tate

USER EVALUATION OF REPORT

Please take a few minutes to answer the questions below; tear out this sheet and return it to Director, US Army Ballistic Research Laboratory, ARRADCOM, ATTN: DRDAR-TSB, Aberdeen Proving Ground, Maryland 21005. Your comments will provide us with information for improving future reports.

1. BRL Report Number _____

2. Does this report satisfy a need? (Comment on purpose, related project, or other area of interest for which report will be used.)

_____

_____

_____

3. How, specifically, is the report being used? (Information source, design data or procedure, management procedure, source of ideas, etc.) _____

_____

_____

4. Has the information in this report led to any quantitative savings as far as man-hours/contract dollars saved, operating costs avoided, efficiencies achieved, etc.? If so, please elaborate.

_____

_____

5. General Comments (Indicate what you think should be changed to make this report and future reports of this type more responsive to your needs, more usable, improve readability, etc.) _____

_____

_____

_____

6. If you would like to be contacted by the personnel who prepared this report to raise specific questions or discuss the topic, please fill in the following information.

Name: _____

Telephone Number: _____

Organization Address: _____

_____

_____